

HELIUM DIFFUSION RATE, PERMEATION RATE, AND
ACTIVATION ENERGY FOR POLYCRYSTALLINE ALUMINA

A THESIS


Presented to
the Faculty of the Graduate Division
by

James Joseph Hurst, Jr.

In Partial Fulfillment
of the Requirements for the Degree
Master of Science in Ceramic Engineering

Georgia Institute of Technology

December, 1961



"In presenting the dissertation as a partial fulfillment of the requirements for an advanced degree from the Georgia Institute of Technology, I agree that the Library of the Institution shall make it available for inspection and circulation in accordance with its regulations governing materials of this type. I agree that permission to copy from, or to publish from, this dissertation may be granted by the professor under whose direction it was written, or, in his absence, by the dean of the Graduate Division when such copying or publication is solely for scholarly purposes and does not involve potential financial gain. It is understood that any copying from, or publication of, this dissertation which involves potential financial gain will not be allowed without written permission.

✓

"

HELIUM DIFFUSION RATE, PERMEATION RATE, AND
ACTIVATION ENERGY FOR POLYCRYSTALLINE ALUMINA

June 5, 1962

ACKNOWLEDGEMENTS

The author wishes to express his thanks to Dr. Willis E. Moody, School of Ceramic Engineering, Georgia Institute of Technology, for his valuable assistance and guidance in the course of this investigation. He is also indebted to Dr. Lane Mitchell, Dr. Niels Engel, and Mr. Thomas Mackrovitch, of the Georgia Institute of Technology.

The financial aid of the Georgia Institute of Technology and the Atomic Energy Commission is gratefully acknowledged.

The author wishes to express his sincere appreciation to his parents for their assistance.

TABLE OF CONTENTS

	Page
ACKNOWLEDGMENTS	ii
LIST OF TABLES	v
LIST OF ILLUSTRATIONS	vi
SUMMARY	viii
CHAPTER	
I. INTRODUCTION	1
II. REVIEW OF LITERATURE	2
Helium Gas	2
Alumina Structure	2
Nature of the Polycrystalline Solid	8
Transport of a Gas Through A Solid	10
The Molecular Flow Processes	12
Diffusion Processes	15
Diffusion in Alumina	22
Quantitative Helium Detection	23
III. PROCEDURE	26
General	26
Carborundum Company and Lucalox Alumina	27
Density Determination	29
Specimen Preparation	33
Diffusion Cell	36

TABLE OF CONTENTS (Continued)

	Page
Mathematics of Molecular Flow	42
Mathematics of Diffusion	43
Preparation of Electron Micrographs	46
IV. DISCUSSION OF RESULTS	48
V. CONCLUSIONS	75
BIBLIOGRAPHY	77
APPENDIX A	80
APPENDIX B	81
APPENDIX C	94
APPENDIX D	97

LIST OF TABLES

Table		Page
1.	Properties of Amarillo Grade A Helium	3
2.	Alpha-Alumina Crystal Data	5
3.	Properties of Lucalox Alumina	30
4.	Properties of Carborundum Company Alumina	31
5.	Seal Composition	37
6.	Physical Dimensions of Specimens	49
7.	Physical Dimensions of Specimens Not Completely Studied . .	50
8.	Diffusion Data	57
9.	Experimental Values of the Diffusion Equation	59
10.	Series J. Polycrystalline Specimen 51 Day Run	82

LIST OF ILLUSTRATIONS

Illustration	Page
1. Basal Plane, Al_2O_3	6
2. Aluminum Ion and Hole Distribution in the Simple Hexagonal Lattice	7
3. The Three Basic Mechanisms of Diffusion	16
4. Potential Energy Curve Showing the Activated State . . .	20
5. Mass Spectrometer Tube Schematic	25
6. Mercury Volumeter Schematic	32
7. Faceting Goniometer and Diamond Lapping Wheel	34
8. Ultrasonic Impact Grinder	35
9. Assembled Test Specimens	38
10. Diffusion Cell Schematic	39
11. Plane Membrane Diffusion	44
12. Specimen Data Series D	51
13. Specimen Data Series E	52
14. Specimen Data Series F	53
15. Specimen Data Series G	54
16. Specimen Data Series H	55
17. Specimen Data Series J	56
18. Helium Diffusion in Alumina	60
19. Calculated Activation Energies	61
20. Molecular Flow Data	66

LIST OF ILLUSTRATIONS (Continued)

Illustration	Page
21. Electron Micrograph of Lucalox Alumina	69
22. Electron Micrograph of Carborundum Company Alumina . . .	70
23. Electron Micrograph of Carborundum Company Alumina. . . .	71
24. Electron Micrograph of Carborundum Company Alumina	72

SUMMARY

The purpose of this study was to investigate, in the temperature range 25°C to 1000°C, the diffusion mechanism by which an inert gas, helium, passes through polycrystalline alumina, Al_2O_3 . In the course of this investigation, the diffusion coefficient and activation energy for helium passing through polycrystalline alumina were determined. Only limited information has been obtained on helium diffusion through polycrystalline alumina at temperatures below 1000°C. Bulk densities of the samples investigated were obtained, and a correlation was made between the physical characteristics of the samples and the diffusion constants.

The diffusion barriers were formed to the desired dimensions from polycrystalline blanks. Two dense polycrystalline tubes were sealed to opposite sides of the diffusion barrier with a high temperature seal. The assembled test specimen was installed in a controlled atmosphere furnace designed to effect a vacuum of 10^{-5} mm. Hg on one side of the barrier while one atmosphere of helium was maintained on the other side. With a controlled temperature system, measurements of the specimen leak rate and temperature were made over the temperature range 25°C to 1000°C. The high vacuum side of the barrier was continually pumped and sampled with a mass spectrometer.

Experimental evidence indicates that the coefficient of diffusion of helium gas through polycrystalline alumina could be measured in the temperature range 300°C to 1000°C with a mass spectrometer.

It was determined that the coefficient of diffusion varied from 10^{-11} cm.²/sec. to 10^{-7} cm.²/sec. for barrier thicknesses of 0.18 cm. to 0.076 cm. Very little or no correlation was noted between diffusion coefficient and bulk density for densities in the range 3.70 gm./cm.³ to 3.90 gm./cm.³. Samples of polycrystalline alumina containing small amounts of MgO and closely approaching theoretical density yielded no measurable results in the temperature range 25°C to 1000°C. The experimentally determined activation energies for the lower density alumina, 0.222 ev., 0.414 ev., and 0.830 ev. indicated that the probable basic mechanism of diffusion was atom-vacancy interchange along grain boundaries with the possibility of small amounts of interstitial diffusion.

One specimen was found to exhibit helium flow characteristics different from the other samples investigated. From experimental data obtained, the probable flow was not a diffusion but rather a molecular flow process which degenerated from a laminar to a turbulent flow.

CHAPTER I

INTRODUCTION

The use of high alumina ceramics has increased greatly in all fields in the last several years. Unfortunately, basic information concerning its properties has not kept pace because of difficulties of experimental techniques for making measurements.

The purpose of this study was to investigate the diffusion mechanism for an inert gas, helium, as it passes through polycrystalline alumina, in the temperature range 25°C to 1000°C . A study of the diffusion rate, as a function of the bulk density of the alumina, was made. The measurement of the coefficient of diffusion at various temperatures made it possible to determine the activation energy and mechanisms of diffusion.

Other mechanisms of molecular flow were considered on certain specimens when it became obvious that high flow rates and a rapid equilibrium state were obtained.

CHAPTER II

REVIEW OF THE LITERATURE

Helium Gas

Helium gas is the lightest of all the inert gas series and remains atomic, rather than assuming a molecular configuration, in the gaseous state. It has an atomic radius of 0.93 \AA , which approximates the size of many metal atoms and other types of ions. It has been suggested (1) that helium will not diffuse through the close-packed structure of some metals because of a lack of chemical affinity. Detecting instruments of a greater sensitivity than have previously been used could clarify this point.

In the case of the more open lattice structures, typical of which are ceramic oxides, diffusion of gases has been found to be a function of the atomic size if no chemical affinity exists (2).

Table 1 lists the properties of the helium gas used in this work.

Alumina Structure

The compound $\alpha\text{-Al}_2\text{O}_3$ falls into a general group designated by the form R_2O_3 . In this group, there is a definite gradient of sizes of the metal ions composing the compounds. In general, the greater the charge on the ion, the smaller will be its atomic radius. With small metal atoms that have $r_{\text{R}}/r_{\text{O}}$ less than 0.60, oxygen ions can approach nearer to a close-packing, and such metallic and close-packed sesquioxides

Table 1. Properties of Amarillo Grade A Helium (3), (4)

Atomic Number	2	
Atomic Weight	4.003	
Melting Point	-272.2°C	(26 atmospheres)
Boiling Point	-268.9°C	(1 atmosphere)
Purity	99.99 ⁺ %	
Purity Measurement	Mass Spectrometer	
Chief Impurities	H ₂ , Ne, N ₂ , O ₂ , A, CO ₂	(18.2 ppm. total)
Atomic Radius	0.93 Å	
Atomic Velocity at 300°K	1.252 X 10 ⁵ cm./sec.	
Atomic Velocity at 600°K	1.920 X 10 ⁵ cm./sec.	
Atomic Velocity at 900°K	2.360 X 10 ⁵ cm./sec.	

are often found in the arrangement typified by Cr_2O_3 . Its symmetry is rhombohedral with a unit cell containing two molecules and having dimensions given in Table 2. The space group is $D_{3d}^6(R\bar{3}c)$, and the atoms are in the following positions (5):

R:	(c)	(u, u, u)	(\bar{u} , \bar{u} , \bar{u})	B. C.
O:	(e)	(v, \bar{v} , 0)	(\bar{v} , 0, v)	(0, v, \bar{v})
		($1/2 - v$, $v + 1/2$, $1/2$)	($1/2 - v$, $1/2$, $v + 1/2$)	
		($1/2$, $1/2 - v$, $v + 1/2$)		

For $\alpha\text{-Al}_2\text{O}_3$, u is listed as 0.105, and v as 0.303 (See Figure 1).

In this structure, each aluminum ion has three oxygen ions at a distance of 1.89 Å and three more at 1.93 Å. The nearest O-O distance is 2.49 Å.

This arrangement is probably best viewed as a slightly distorted hexagonal close-packing of molecules in which aluminum ions occur above and below the midpoints of oxygen ion triangles of the close-packed oxygen layers. Six oxygen ions surround each aluminum ion, and each oxygen ion is surrounded by four aluminum ions. Two-thirds of the octahedral sites are occupied by aluminum ions while the remaining ones are vacant to fulfill the conditions of net electrical neutrality and stoichiometry of the compound. Aluminum ions and holes are arranged so as to give a maximum separation of like charges and a minimum separation of unlike charges (6), (7), Figures 1 and 2. The packing would be theoretically perfect if α were $53^\circ 47'$ instead of $55^\circ 17'$ and if all the oxygen ions were equidistant from the aluminum ions (8).

Figure 1 represents a plan view of the $\alpha\text{-Al}_2\text{O}_3$ structure looking down on the aluminum ions and holes over the close-packed oxygen ion

Table 2. Alpha-Alumina Crystal Data (9)

Form	alpha-Al ₂ O ₃
Structure	Cr ₂ O ₃ type
Symmetry	Rhombohedral
a _o	4.76280 Å
b _o	not defined
c _o	13.00380 Å
α	31°
Coordination Number Al to O	6 : 4
Dislocation Annealing Temperatures	900°C Basal Plane 2000°C Prismatic Plane
Melting Point	2050°C
Parting	Rhombohedral Plane
Slip	Basal and Prismatic Planes

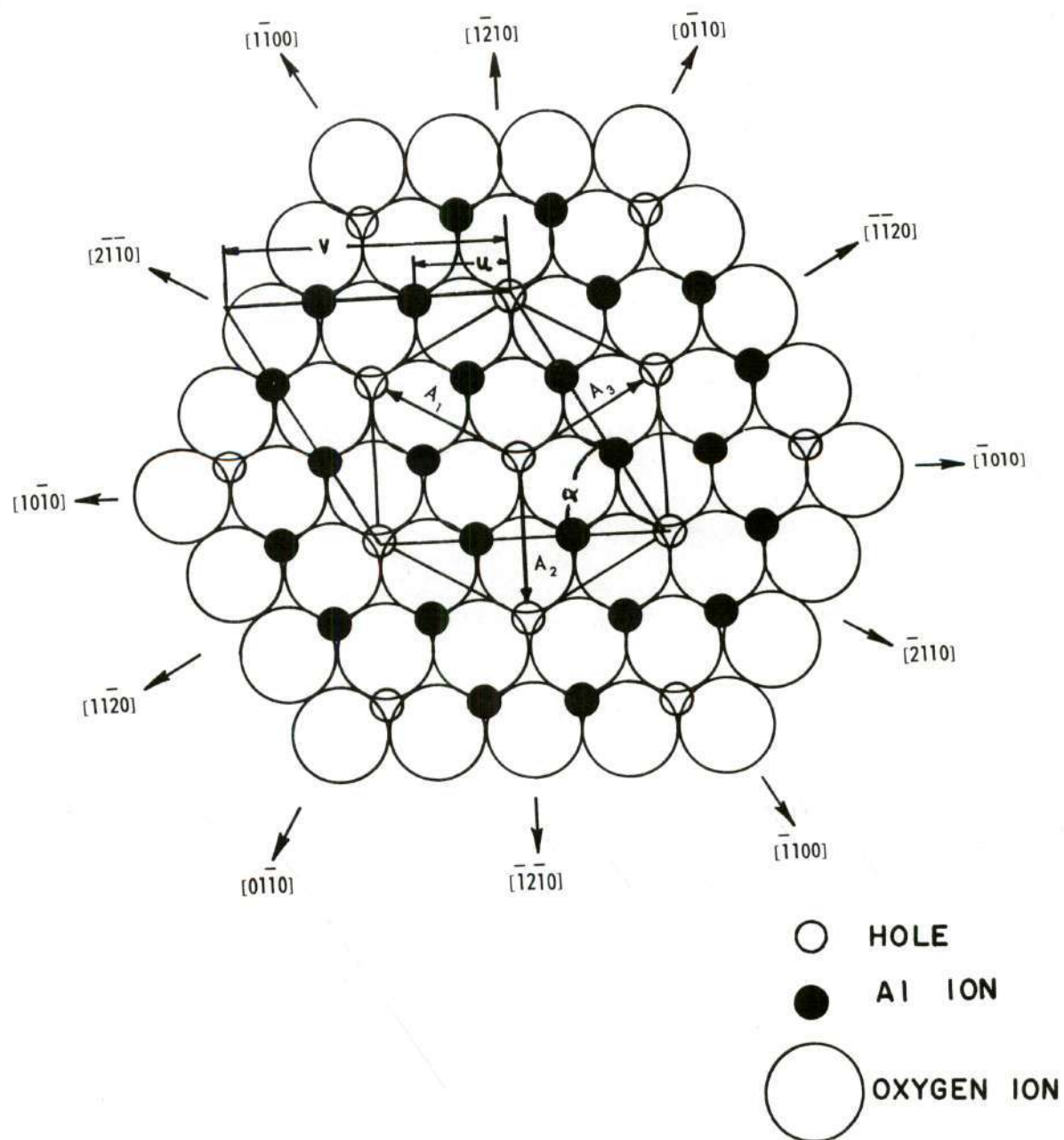


Figure 1. Basal Plane, Al_2O_3 (10).

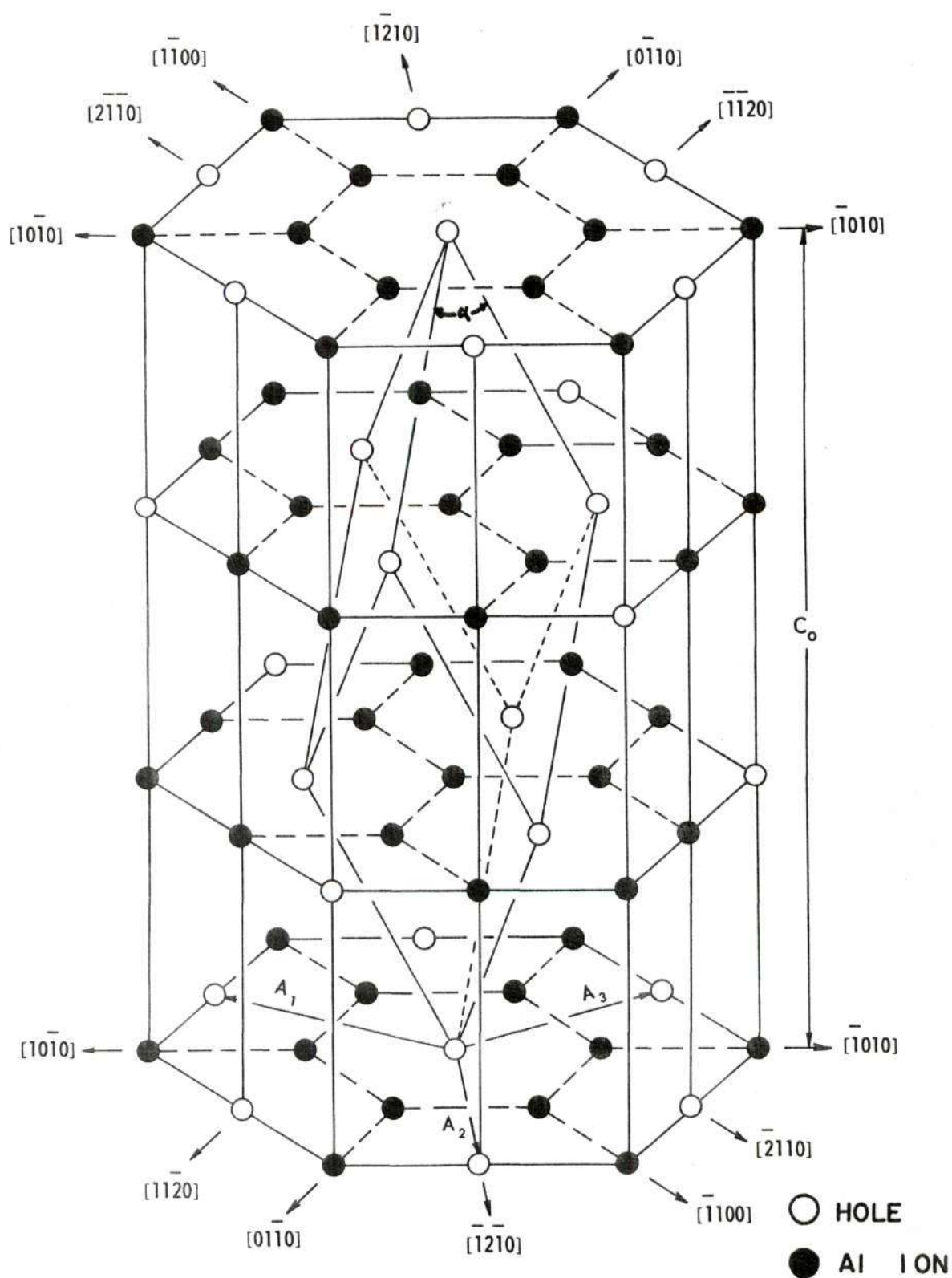


Figure 2. Aluminum Ion and Hole Distribution in the Simple Hexagonal Lattice (11).

layer. Figure 2 shows a schematic diagram of the aluminum ion and hole distribution in a simple hexagonal lattice. For any gas penetration to take place, some sort of activated, step-by-step diffusion process would be necessary to supply the energy for motion.

Several other forms of alumina are found in nature or occur through artificial means. Beta and Zeta forms contain small amounts of alkali and alkaline earth oxides. Gamma types, of which there are many subdivisions (chi, gamma, eta, delta, kappa, theta), all are structures that originally contained water and revert to the alpha form upon heating (12). Studies thus far reveal that the alpha crystalline form is stable from room temperature to 2000°C and exhibits no inversions or phase transformations upon heating (13).

Nature of the Polycrystalline Solid

Highly calcined or sintered alumina, electric furnace or fused alumina, and natural corundum all have identical x-ray diffraction powder patterns. The methods of formation of all are quite different; consequently, the crystal habits vary.

A polycrystalline material behaves quite differently from its single crystal counterpart. There are several reasons for this lack of correspondence. The presence of internal surfaces, or grain boundaries, and external surfaces can greatly affect the various properties of a solid.

Grain boundaries may be defined as unordered regions of atoms between two lattices. Essentially they may be thought of as internal surfaces since they have surface energy that appears in the form of surface tension. These surfaces may be formed in many ways. Recrystallization

of a solid, cooling from a melt, or by sintering and interdiffusion from an aggregate are some of the more common methods of formation. The variety of the methods of formation does not necessarily mean that there are differences in the boundaries generated. In all cases they represent regions of misfit between two or more crystalline surfaces. The atoms in the boundary region are shared by adjacent lattices, but the force field in which the atoms find themselves is by no means uniform, and the region is in stress and permanent strain. Generally, a grain boundary is at a higher potential energy state than its surroundings. There is experimental evidence for this. The grain boundary region is attacked first in the etching of a polycrystalline solid. Melting point studies indicate that grain boundaries melt before the matrix material. Finally, diffusion studies show that atoms move along grain boundaries at a rate many orders of magnitude higher than through the crystal lattice (14).

The term "sintered" alumina became established in the literature in 1932 when Kohl described a new material called "sinterkorund" made from a Bayer alumina material either by slip casting or dry pressing and fired to 1800°C. He considered the firing and cooling step to be a recrystallization process.

Sintering, unfortunately, is a term that is widely used by little understood. It has previously been defined as a process which decreases the porosity of a material by partial fusion. A pure crystalline oxide could not sinter under these conditions. It would either fuse or remain in its original state. Studies of this phenomenon in the fields of ceramics and glasses now reveal sintering to be a process of atomic diffusion in the solid state through surfaces in contact with each other mechanically (15).

Unlike electric furnace products, in which crystals are of primary origin and form from a molten magma, there is a multitude of crystalline centers in the case of a sintered polycrystalline solid (16).

In summation, the properties of a polycrystalline substance, that depend upon or are a function of the ionic bonds, are affected by the presence of a boundary in the sense that the region is a lattice imperfection. It represents a discontinuity in the potential field, but it is not a barrier that completely blocks electronic interchange. Mechanical properties depend upon ionic movements, and grain boundaries represent areas sufficiently different to modify the behavior of the material (17), (18).

Transport of a Gas through a Solid

There are many ways by which a gas may penetrate a solid. A solid usually exhibits properties favoring several types of penetration simultaneously.

The simplest case occurs when the solid is porous--when there are holes in the material of such an order of magnitude that the gas does not even see the material through which it is passing. The pores are interconnected so that a large free path exists. An insulating refractory is a good example of a material of this type.

If the path diameter is reduced to an order of magnitude that is greater than the atomic diameter of the gas, but on the order of a capillary tube, certain other effects are introduced to the transport phenomena. The gas moving through the capillary meets resistance to flow because of atoms rebounding from the walls, and end effects (19).

The most energetic process is that of a diffusion mechanism. Here the path diameter has been reduced to an order of magnitude comparable to the size of the diffusing particle. The process requires that the atom, ion, or molecule possess energy sufficient to push itself through a physical barrier with a potential energy field.

The diffusion of an ion through an ionic solid would represent a situation quite different from that of a neutral atom diffusing through the same material. Atomic diffusion in a relatively open lattice structure should be a function of the concentration gradient and the temperature of the material. The concentration gradient would supply the driving force, and the temperature would control the path size and mechanism of diffusion. A diffusing atom and a diffusing ion of the same atomic diameter should behave quite differently in the same material. The ion would be both attracted and repelled by the charges on the ions in the lattice. It could be easily trapped in vacant lattice sites in the material through which it was passing. Ionic diffusion would be a much more difficult process than atomic diffusion in a relatively open lattice structure.

It has been suggested that inert gas atoms will not diffuse through the close-packed structure of many metals because of a lack of chemical affinity. This would mean that the gas would have to be ionized before it would go into the structure of the metal. If it were not ionized it would not be attracted and nothing would go into solution. Special means would be necessary to drive the neutral atoms into the lattice. However, imperfections such as dislocations or other surface conditions may provide adequate entrance sites for atoms or ions to enter the close-packed

structure. It should be pointed out that the conditions necessary for an atom or an ion to pass through the theoretical surface are not well understood or defined.

The Molecular Flow Processes

Molecular flow processes have been reviewed by Barrer (20) and are of four major types:

Molecular Effusion.--Through an orifice of area A with a diameter small compared to the mean free path of the gas, the number of molecules effusing in a unit time is given by the kinetic theory equations:

$$\frac{dN}{dt} = \frac{A N_0 (p_1 - p_2)}{\sqrt{2\pi MRT}} \quad (1)$$

where N_0 is Avogadro's number, M is the mass of a mole of the material, R is the gas constant, T is the absolute temperature, and $(p_1 - p_2)$ the pressure differential.

Molecular Streaming, or Knudsen Flow (21).--When the path is of considerable length molecules or atoms will collide with its walls on the way through. If all the collisions were perfectly elastic, the flow through the tube would be identical with the effusion velocity through a thin plate. It would be independent of the tube length, which Knudsen proved was contrary to experiment. Knudsen, therefore, supposed that for N molecules striking the wall a fraction f was emitted with a random velocity distribution, and $(1-f)$ were specularly reflected. Some are returned in the direction from which they came and more return the greater length of

the tube. Knudsen showed that the net rate of flow in molecules or atoms per second is given by:

$$\frac{dN}{dt} = \frac{1}{2} B \frac{1}{\sqrt{2\pi MR}} \left(\frac{p_1}{\sqrt{T_1}} - \frac{p_2}{\sqrt{T_2}} \right) \frac{1}{L} \left(\frac{2-f}{2} \right) \quad (2)$$

where L is the length of the tube. B is a constant dependent upon the shape of the tube. For a capillary tube of circular cross-section the constant B takes on the value $\frac{16\pi r^3}{3}$ where r denotes the radius of the capillary.

Poiseuille or Streamline Flow.---For a compressible fluid obeying the perfect gas law, Poiseuille's law may be written:

$$\frac{dN}{dt} = \frac{16r^4\pi}{128 L} \int \frac{1}{\eta R T} p \, dp \quad (3)$$

where η is the viscosity of the fluid, which for an isothermal process with $\eta = \text{a constant}$ becomes:

$$\frac{dN}{dt} = \frac{16r^4\pi}{128 L \eta} \left(\frac{1}{R T} \right) \left(\frac{p_1^2 - p_2^2}{2} \right) \quad (4)$$

This may also take the form:

$$\frac{dN}{dt} = \frac{16 r^4 \pi}{128 \eta R T L} \bar{p} (p_1 - p_2) \quad (5)$$

where $\bar{p} = \frac{1}{2}(p_1 + p_2)$ is the mean pressure in the tube. Also:

$$\frac{dN}{dt} = \frac{16 r^4}{128 L M} \frac{\bar{p}}{\eta} (p_1 - p_2) \quad (6)$$

since $\left(\frac{p_1 + p_2}{2} \right) \frac{M}{R T} = \bar{p}$, the mean density of the gas.

Two corrections may be applied to Poiseuille's formulas. Only part of the pressure difference is used to overcome friction, a fraction which must be subtracted from the original pressure difference produces kinetic energy of motion.

In the boundary layer of gas, of thickness λ , equal to the mean free path, there may be specular reflection from the surface of the capillary. The coefficient of slippage is then $\left[\frac{2-f}{2} \right] \lambda$.

Barrer applies corrections which result in:

$$\frac{dN}{dt} = \frac{1}{L} \cdot \frac{3 \pi^2 r^3}{4} \cdot \frac{1}{2 \pi M R T} \cdot (p_1 - p_2) \cdot \left(\frac{2-f}{2} \right) \quad (7)$$

which is the equation for molecular streaming, except for the numerical constants which are somewhat different.

Turbulent Flow.--Streamline flow changes when a certain limiting mass velocity, ω , is reached. A quantity R , called the Reynolds Number, is defined by:

$$R = \frac{r_h \omega \rho}{\eta} \quad (8)$$

where r_h is the so-called hydraulic radius defined by the ratio of the

cross-section
periphery which for tubes of a circular cross-section is one-eighth of the radius r . The symbols ρ and η have the significance of fluid density and viscosity respectively. It has been determined for circular tubes that streamline equations do not hold when R is greater than 580. The differential equation of flow is:

$$-\frac{dp}{dx} = \frac{\beta \rho \omega^2}{2r_h} \quad (9)$$

where β is a constant and varies for different shapes of tubes.

Diffusion Processes

There are three classical mechanisms by which an atom or an ion may diffuse through a crystal. They are shown in Figure 3 and are as follows (22):

- 1) Atom A and atom B may interchange places. They would move past each other in the lattice to reach the new sites.
- 2) Atom B may diffuse through interstitial sites in the lattice.
- 3) The diffusing atom may move by occupying vacant sites in the lattice.

The first mechanism involves breaking the bonds which surround atoms A and B. This requires an energy equal to the binding energy of the material and is the most unlikely to occur. Experimental evidence seems to uniformly support this assumption.

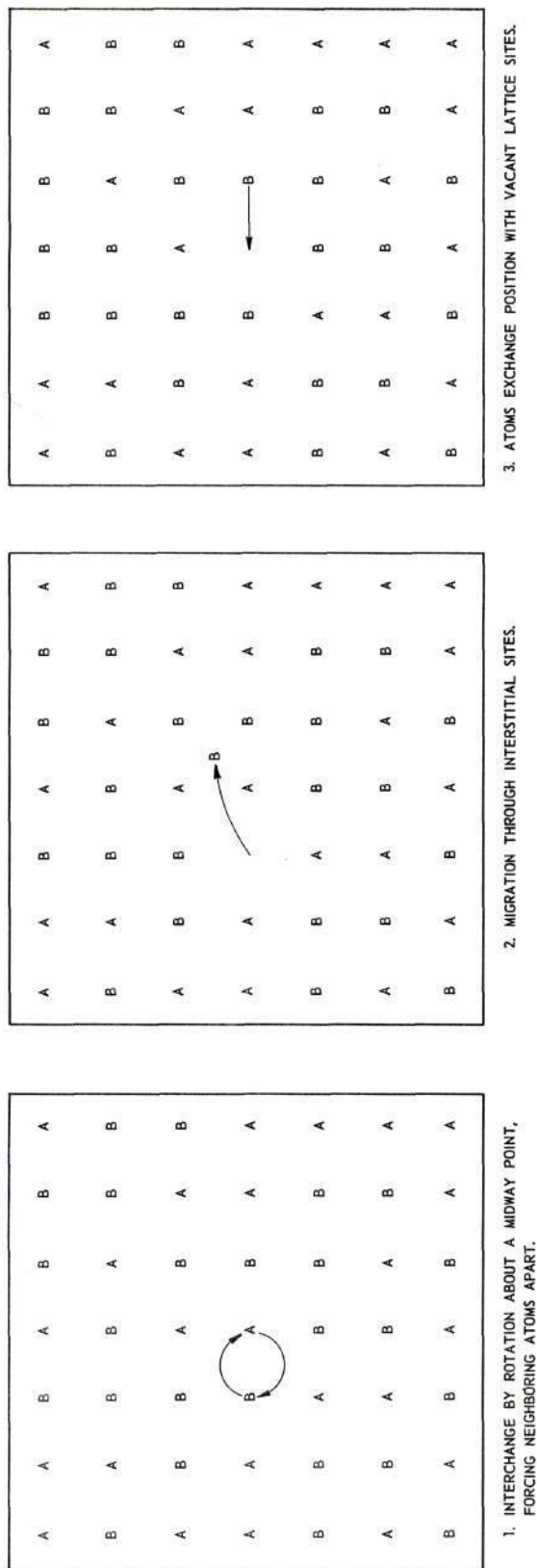


Figure 3. The Three Basic Mechanisms of Diffusion (23).

The second mechanism involves a smaller amount of energy, but the number of interstitial sites available usually limits the process. The ion simply moves out of its equilibrium site into the interstitial position. This is accompanied by some lattice distortion due to the size of the ions and ion-ion energy interaction.

The mechanism requiring the least amount of energy is shown in part three of Figure 3. Crystals usually possess vacant lattice sites or missing atoms or ions, and these would be available as vacancies. It is necessary to overcome binding forces on three sides of the atom to be moved. The new site is available with little additional energy expenditures.

In polycrystalline materials where grain boundaries represent areas of unequal energy potential, but not actual holes, small amounts of energy supplied to a diffusing atom could cause the area to become a diffusing path. Grain boundaries may also consist of holes in which the diffusing path is well defined.

Mathematics of Diffusion.--To fully appreciate the mathematics of diffusion, one must have a working knowledge of kinetics, thermodynamics, solubility phenomena, and steady and non-steady state flow. Numerous references are given in the literature dealing with mathematical solutions of various systems that might be employed, such as plane surfaces, cylinders, and spheres.

The basis for the mathematics of diffusion lies with the two differential forms of Fick's Laws (24) dealing with steady and non-steady state flow. They may be written:

$$J = - D \frac{\partial C}{\partial X} \quad (10)$$

where J = current density, or quantity of substance passed per unit area per unit time per unit thickness

D = diffusion coefficient

$\frac{\partial C}{\partial X}$ = concentration gradient.

Fick's second law may be derived from the first with the use of the particle continuity equation which results in:

$$\frac{\partial C}{\partial t} = D \frac{\partial^2 C}{\partial X^2} \quad (11)$$

where $\frac{\partial C}{\partial t}$ = change of concentration with change in time

$\frac{\partial^2 C}{\partial X^2}$ = rate of change of concentration gradient.

In equations (10) and (11) the term D has been found to be dependent upon such variables as temperature, concentration, orientation of the specimen, and composition. The above equations have been written in the form of partial differentials, with X , Y , and Z components. In an isotropic medium, or for diffusion in one direction only, the Y and Z components may be neglected and exact differentials substituted.

It has been experimentally determined that for very small concentrations, values of D may be expressed by a relation of the following form:

$$D = D_0 \exp(- E_a / k T) \quad (12)$$

where D_0 = diffusion constant

E_a = activation energy

k = Boltzmann constant

T = absolute temperature.

Activation Energy.--The activation energy of a system may be defined as the energy that must be put into the system in order to start a reaction, rearrange a structure, or shift atoms. The rate at which diffusion takes place is a function of the activation energy for the particular diffusion mechanism.

If the natural logarithm is taken of equation (12), an arithmetic plot of $\ln D$ versus $1/T$ will yield a straight line. The magnitude of the slope of the line will be a function of the activation energy and the Boltzmann constant. Thus:

$$\ln D = \ln D_0 - E_a/k 1/T \quad (13)$$

Figure 4 shows a schematic representation of a barrier that has to be overcome by the activation energy.

The Diffusion Constant.--Previously, there have been many values of the diffusion constant published in the literature. This wide range of values was accepted with little speculation as to the significance of the value of D_0 . Zener (25) approached the problem of evaluating D_0 in the following manner.

The normal diffusion equation for small concentrations is given by equation (12). D may also be described by the three dimensional random walk problem:

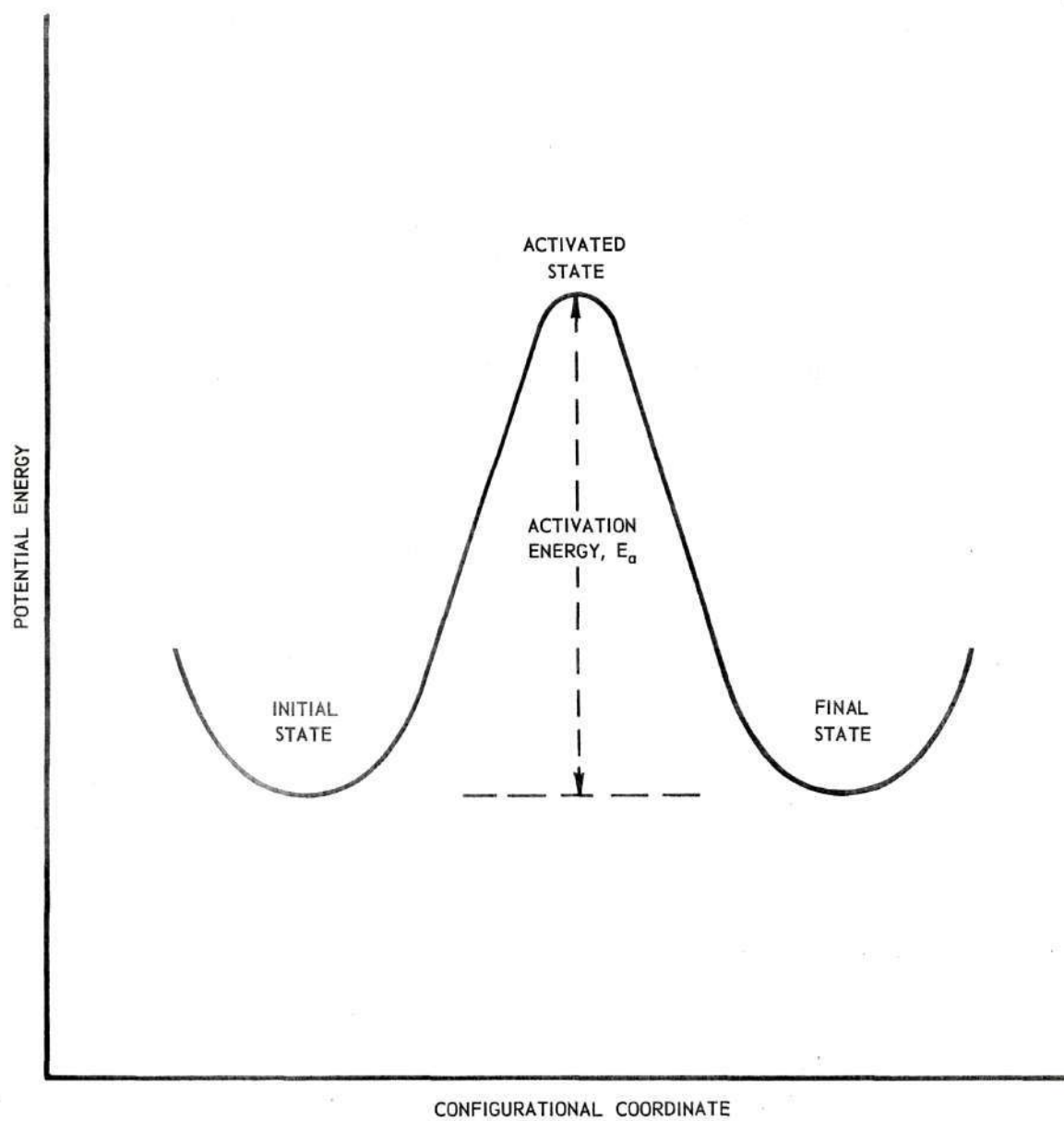


Figure 4. Potential Energy Curve Showing the Activated State.

$$D = 1/6 \sum_i T_i \delta l_i^2 \quad (14)$$

where T_i is the rate at which a jump is made of type i , and δl_i is the jump distance. The crux of the problem of evaluating D_0 lies in the definition of T_i .

T_i may be expressed by:

$$T = v e^{-\Delta G/k T} \quad (15)$$

where v is the frequency of vibration leading to the saddle point, and ΔG is the isothermal work done in moving across the saddle. The constant k is the Boltzmann constant and T is the absolute temperature at which the potential barrier exists.

We separate ΔG into its components by:

$$\Delta G = \Delta H - T \Delta S \quad (16)$$

$$\text{From thermodynamics: } \Delta H = d [\Delta G/T] d(1/T) \quad (17)$$

$$\text{We define: } H/k = - d \ln D/d(1/T) \quad (18)$$

Thus equation (18) may be written in component form:

$$T = v e^{\Delta S/k} e^{-H/k T} \quad (19)$$

$$\text{with } \Delta S = - d \Delta G/d T . \quad (20)$$

Equation (20) may now be examined on the right side. Formerly ΔS was considered to take on values either plus or minus; plus corresponding

to a loosening of the lattice and minus corresponding to a tightening of the lattice. Equation (20) does not allow for this. The value of ΔG does not increase with temperature, at least it is unlikely; and this casts doubts upon experiments with negative values of ΔS and consequently D_0 . The above derivation assumes that all lattice sites are equivalent.

When the matrix is not homogeneous the possibility exists that there are certain paths along which diffusion will have a lower energy of activation than through the bulk of the matrix.

Since at any one time only a fraction of the atoms will be in this path, the associated D_0 will be lower than the value that corresponds to homogeneous diffusion. If the major portion of the diffusion occurs along these paths, ΔS may be smaller than theoretical and may even be negative.

In this manner, low or even negative values of D_0 may be explained by inhomogeneities which furnish short-circuit diffusion paths. Grain boundaries are a major source of such paths along with dislocations. Zener postulates that if these inhomogeneous areas were removed, values of ΔS would become positive and values of D_0 would fall around 10^{-2} cm.²/sec. according to the theory.

Diffusion in Alumina

Studies on the penetration of gases in polycrystalline alumina have been conducted recently by several sources. Campbell (26), Hayes, et al. (27), and Kingery, et al. (28) have investigated this phenomenon from 25°C to 1800°C.

Campbell found that in the temperature range 25°C to 900°C, the probable mechanism of diffusion of helium in polycrystalline alumina was

that of an atom vacancy type along grain boundaries. Measurements were made with a helium mass spectrometer.

Hayes, et al., working in the temperature range 25°C to 1700°C, with oxygen, nitrogen, and argon as the diffusing gases, found that a combination of Knudsen flow and activated diffusion along the grain boundaries was the probable mechanism. They also found that the elevated temperatures greatly shortened the life of the alumina, and a massive breakdown of structure occurred. The samples employed by Hayes were of a lower density than those examined by Campbell, and the method of analysis was based upon pressure buildup techniques rather than a diffusion product analysis for oxygen gas. No results were obtained for argon diffusion, and the experimental data obtained for nitrogen diffusion was not reproducible.

Kingery, et al., studied the self diffusion of O^{18} in the lattice of single and polycrystalline alumina and found the probable mechanism of diffusion to be movement along holes produced by defects. They found the diffusion rate through polycrystalline alumina to be somewhat higher and with a slightly lower activation energy when compared with single crystals. They made no assumptions from the data regarding ion-ion interaction. At temperatures less than 1450°C variable results were obtained, possibly due to structure sensitive diffusion. At higher temperatures, grain boundary diffusion played an important role.

Quantitative Helium Detection

A mass spectrometer is used for the quantitative detection of small amounts of a gas. The sample is ionized and driven by an electrical

potential through a magnetic field which deflects it. The magnitude of the deflection is dependent upon the atomic weight of the ion. Standard deflection values are set up for qualitative analysis. By measuring the quantity of an unknown sample caught on the collector, in terms of an electrical output and comparing it with the output of a known sample, a quantitative analysis may be determined. The detection limits, or sensitivity, of a typical instrument is one part of helium in ten million parts of air. A schematic drawing of a mass spectrometer tube is shown in Figure 5.

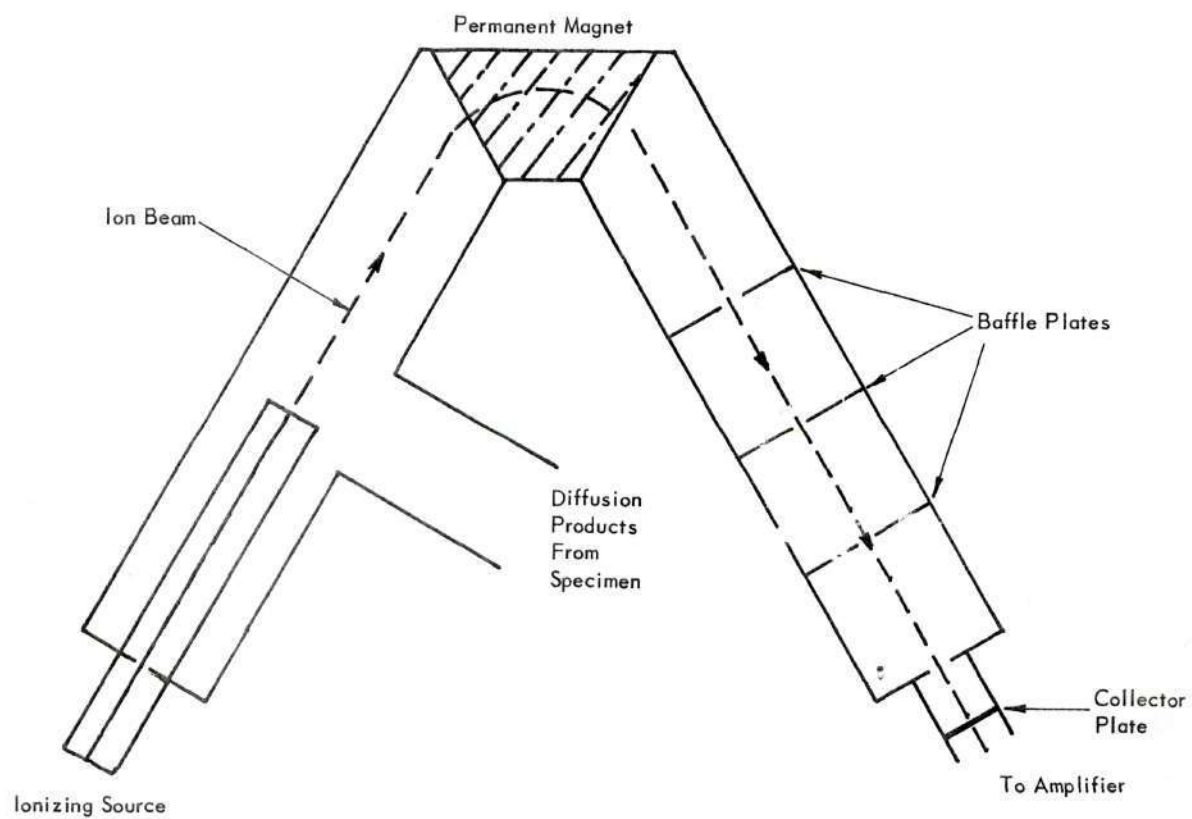


Figure 5. Mass Spectrometer Tube Schematic.

CHAPTER III

PROCEDURE

General

The specimens were received in the form of sintered polycrystalline blanks, the Lucalox specimens having the exterior profile shaped and the Carborundum Co. alumina samples unshaped. All were thoroughly cleaned in acetone and the bulk density of each specimen was determined with the aid of an analytical balance and a mercury volumeter. Carborundum Co. alumina samples were shaped with a diamond lapping wheel. Barriers for all the samples were formed with an ultrasonic impact grinder. Barriers were leak checked at this point to determine if any structural flaws had been introduced during the forming process.

The second step involved the sealing of the samples between two high density alumina tubes by means of a glass seal. Prior to the application of the seal the samples and tubes were lapped together to insure a tight fit. The samples were fired together in a two stage process. The first step involved the coating of all sealing surfaces with a seal and firing to maturity, and the second step involved the firing of the entire assembly together. All finished samples were leak checked with a helium leak detector.

The assembly was installed into a controlled atmosphere furnace designed to maintain a vacuum of 10^{-5} mm. Hg on one side of the barrier while holding one atmosphere of helium on the other side. Temperature

control was maintained with a resistance heating element powered by a powerstat, or a saturable reactor and temperature controller alternately.

The high vacuum side of the apparatus was continually samples with a mass spectrometer set for the helium peak. Data recorded included leak rate, temperature, and pressure on the high vacuum side of the system.

The data were used to calculate values of the diffusion coefficient and activation energy. Correlation was noted between the diffusion coefficient and the bulk density of various samples.

Carborundum Company and Lucalox Alumina

The fabrication processes of the two types of polycrystalline alumina used in this work were investigated in order to obtain a better insight into the possible diffusion mechanisms.

The first type, from which most of the samples were obtained, was manufactured by the Carborundum Company. It was fabricated by the more standard technique of hot pressing granular alpha-alumina. A graphite die and induction furnace was used, and a controlled sintering schedule was carried out. The original particle size of the granular alumina, about 30μ as an average particle size, the die pressures, and the sintering schedule contribute to the final bulk density of the samples. Typical densities may be seen in Tables 5 and 6. The specimens deviated a maximum of seven per cent from theoretical density and averaged 2.3 per cent lower. Other properties of the material, such as thermal expansion and thermal conductivity, were also governed by the firing cycle.

Crandall (29) reports that Ryachkenitach and Jackman have found that the strength of polycrystalline alumina decreases rapidly in the

temperature range above 900°C. This would make diffusion studies in this region subject to the properties of the individual sample in question.

Lucalox alumina was manufactured by another type of process. It was pressed into the desired shape while at room temperature, and then fired to very high temperatures. The original size of the granules used in this process, about 3μ , was much smaller than the sizes employed in the hot pressing technique. Small amounts of $\text{Mg}(\text{NO}_3)_2$, up to about 0.25%, are usually added, by spraying, to the alumina granules. This coats the granules with a fine film containing the Mg^{++} ion, which changes upon heating to MgO . The addition of small amounts of foreign ions to promote sintering while impeding grain growth has been attempted in the past on other materials, notably beryllia. In many cases, the densities reached may be higher than that of the single crystal counterpart, if the foreign ion works into interstitial sites of the lattice of the material to be sintered; or if the foreign ion forms a compound with the matrix material.

In the case of Lucalox alumina, the Mg^{++} ions are distributed in the following ways. Some of the ions move into vacant lattice sites in the alumina lattice. This movement fills voids that would otherwise be present and increases the density. The greater portion of the Mg^{++} ions reacts with the alumina to form a eutectic that lies at the grain boundaries and melts at 1987°C. This is the lowest melting eutectic in the $\text{MgO-Al}_2\text{O}_3$ system and it causes the 10°C difference between the theoretical alumina melting point (2050°C) and the observed melting point.

The resultant Lucalox is translucent, due to the absence of microscopic pores and bubbles. Light is reflected and dispersed only at grain

boundaries. The density of the material averages 3.98^{\pm} gm. cc.⁻¹, or around the x-ray density of the perfect single crystal. Removal of the microscopic pores had previously been thought impossible (30). Table 3 lists the properties of Lucalox alumina. Table 4 lists the average properties of Carborundum Company alumina.

Density Determination

All density determinations were made with the aid of a mercury volumeter and a standard analytical balance. A schematic diagram of the mercury volumeter used is shown in Figure 6. The temperature at which density determinations were made was 25°C. Mercury, at one atmosphere pressure, will not wet pores in a sample less than 12 microns in diameter. Therefore, any exterior pores present are included in the bulk volume obtained. This is also true for any interior pores that might be present. It has been determined that hot pressed specimens of alumina with densities greater than 3.85 gm. cc.⁻¹ would exhibit no measurable porosity, and there is experimental evidence to support this fact (31).

The density determination was simple. The sample was placed in mercury and under a sample holder with a weighing pan attached. Weights were added until the sample and sample support sank into the mercury to the tare mark on the stem of the support. This weight was recorded. The sample was removed, and the weight necessary to immerse the sample holder in the mercury to the tare mark was recorded. By subtracting the second weighing from the first, the weight necessary to immerse the sample was obtained. This was the actual weight of mercury displaced by the sample.

Table 3. Properties of Lucalox Alumina (32)

Crystal Form	$\alpha\text{-Al}_2\text{O}_3$
Purity	99.9 ⁺ % Al_2O_3
Structure	Polycrystalline
Density	3.98 gm./cm. ³ average
Porosity	Gas Tight, essentially zero
Melting Point	2040°C
Coordination Number of Al to O	6 to 4
Chief Impurity	MgO
Average Grain Size Before Sintering	$\approx 3\mu$
Average Grain Size After Sintering	$\approx 7\mu$

Table 4. Properties of Carborundum Company Alumina

Crystal Form	$\alpha\text{-Al}_2\text{O}_3$
Purity	99.1 ⁺ % Al_2O_3
Structure	Polycrystalline
Density	3.70 to 3.90 gm./cm. ³ average
Porosity	Essentially Zero
Melting Point	2015°C average
Chief Impurity	Na_2O
Average Grain Size Before Sintering	≈ 20 to 30μ
Average Grain Size After Sintering	≈ 40 to 50μ

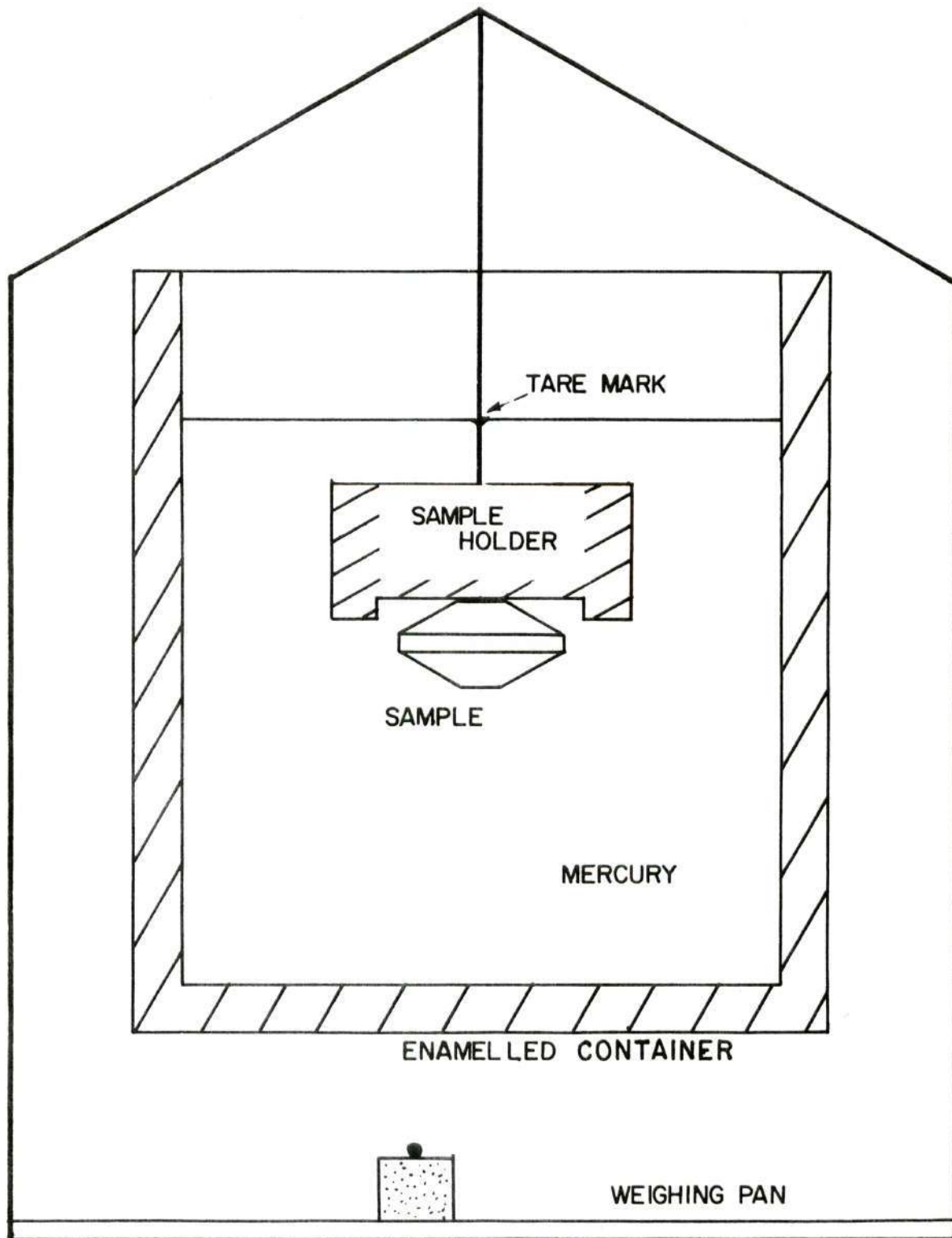


Figure 6. Mercury Volumeter Schematic.

This value plus the sample weight in air divided by the density of the mercury at the weighing temperature gave the volume of the mercury displaced. Consequently, the sample volume was known.

Dividing the sample weight by its volume gave the bulk density of the sample. The formulas involved were:

$$\frac{\text{weight of the sample in Hg} + \text{weight of the sample in air}}{\text{density of Hg at weighing temp.}} = \text{volume of sample} \quad (21)$$

$$\frac{\text{weight of sample in air}}{\text{volume of sample}} = \text{Bulk Density} \quad (22)$$

Densities were remeasured and found to be reproducible to the second decimal place. The measured density of a single crystal specimen was found to be 3.98 gm./cm.³, the expected value.

A sample calculation is given in Appendix B.

Specimen Preparation

The specimens were received in a blank and semi-finished form. The exterior profile of the Carborundum Company alumina samples was shaped with a faceting goniometer made by the M. D. R. Manufacturing Company, Los Angeles, and a 100-mesh diamond lapping wheel, Figure 7. All barriers were formed 0.25 inches in diameter and to the desired thickness with an ultrasonic impact grinder made by the Raytheon Company, model 2-334. The average thickness of each barrier was in the range of fifty-thousandths of an inch, a value that was found to be satisfactory in previous work (33). The abrasive, B₄C, used was supplied by the Norton Company. The impact grinder is shown in Figure 8.

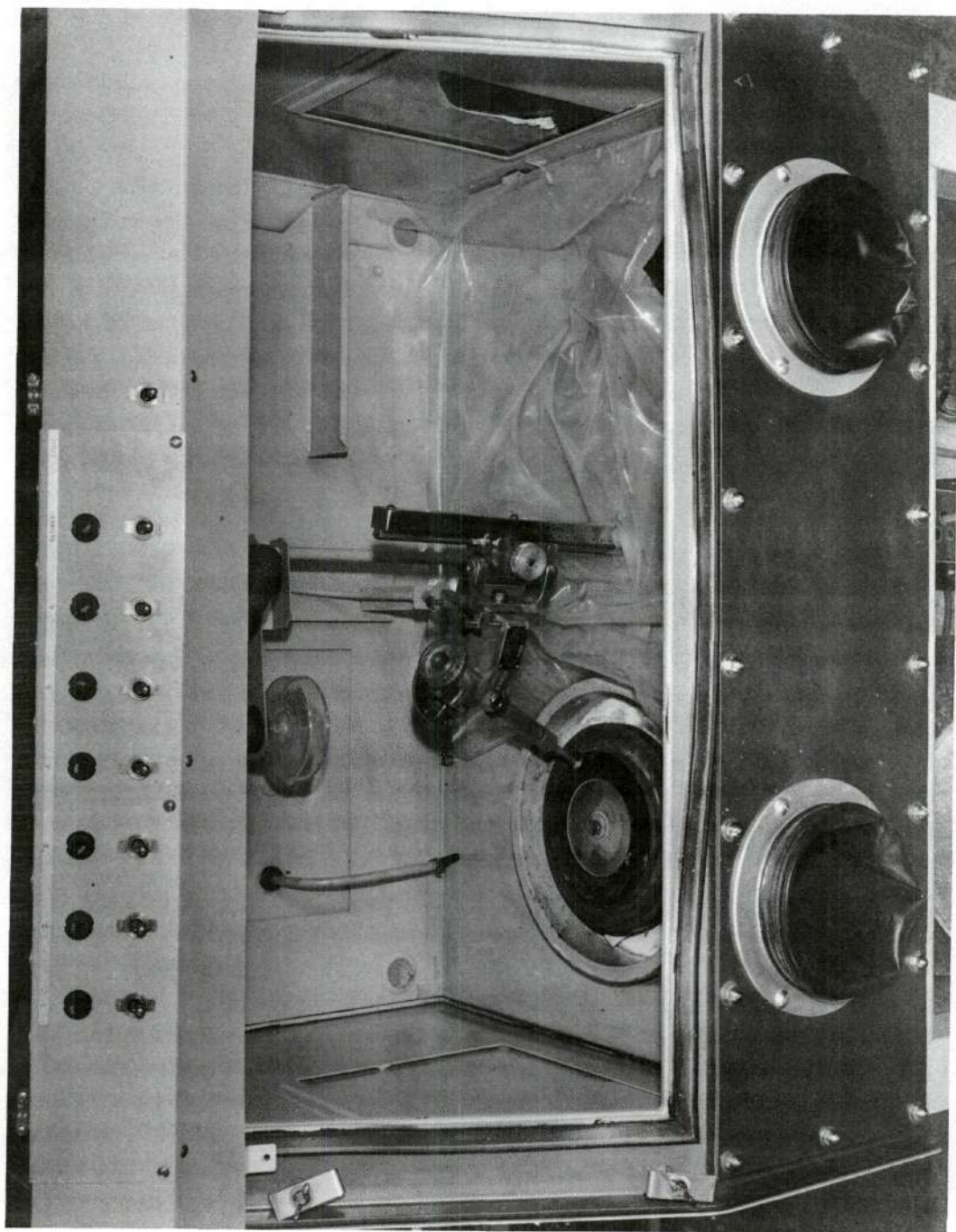


Figure 7. Faceting Goniometer and Diamond Lapping Wheel.

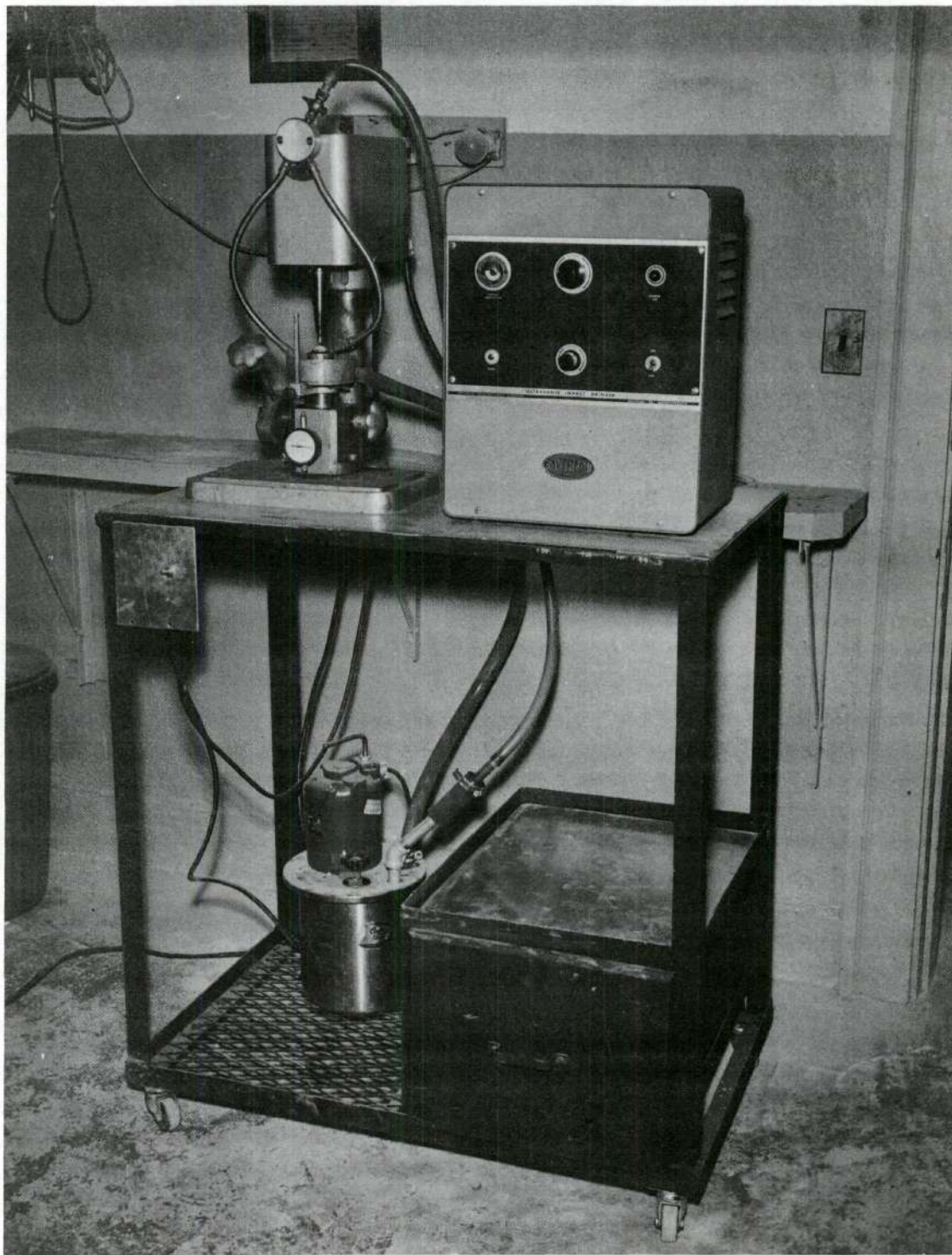


Figure 8. Ultrasonic Impact Grinder.

After the preliminary lapping of the exterior profile was completed, the sample and polycrystalline tubes, into which the sample was to be sealed, were lapped together with boron carbide as the abrasive. The procedure insured a tight mechanical fit.

The polycrystalline tubes employed were of 98 per cent alpha- Al_2O_3 with a 1.50 inch outside diameter, a wall thickness of 0.625 inch, and a length of approximately nine inches. One end of each tube was shaped to the barrier profile, while the other end was flanged to facilitate installation into the diffusion cell.

The assembly was fused in a two stage operation. All seal surfaces were coated with seal composition and matured individually in the first firing. The matured components were then assembled and refired. The maturing temperature for the first firing was 1500°C . The maturing temperature for the final seal was 1515°C , with a one hour soaking period at that temperature. An eight hour firing schedule was employed. Temperature measurements were made with a Pyro Optical Pyrometer, accurate to $\pm 8^\circ\text{C}$. The seal composition is shown in Table 5. Finished and unfinished assemblies are shown in Figure 9.

Diffusion Cell

Figure 10 shows a schematic diagram of the system used in this work. It was designed to operate in pressure ranges on the order of 10^{-5} mm. Hg to a lower limit of 2×10^{-6} mm. Hg. This last figure represents the lower limits of the pressures obtainable with the mass spectrometer pumping station. The other side of the barrier was maintained at one atmosphere pressure of helium. The furnace volume surround the assembly

Table 5. Seal Composition

Empirical Formula in Moles

0.600 CaO

0.200 MgO

0.100 BaO

0.100 SrO

1.30 Al₂O₃13.0 SiO₂

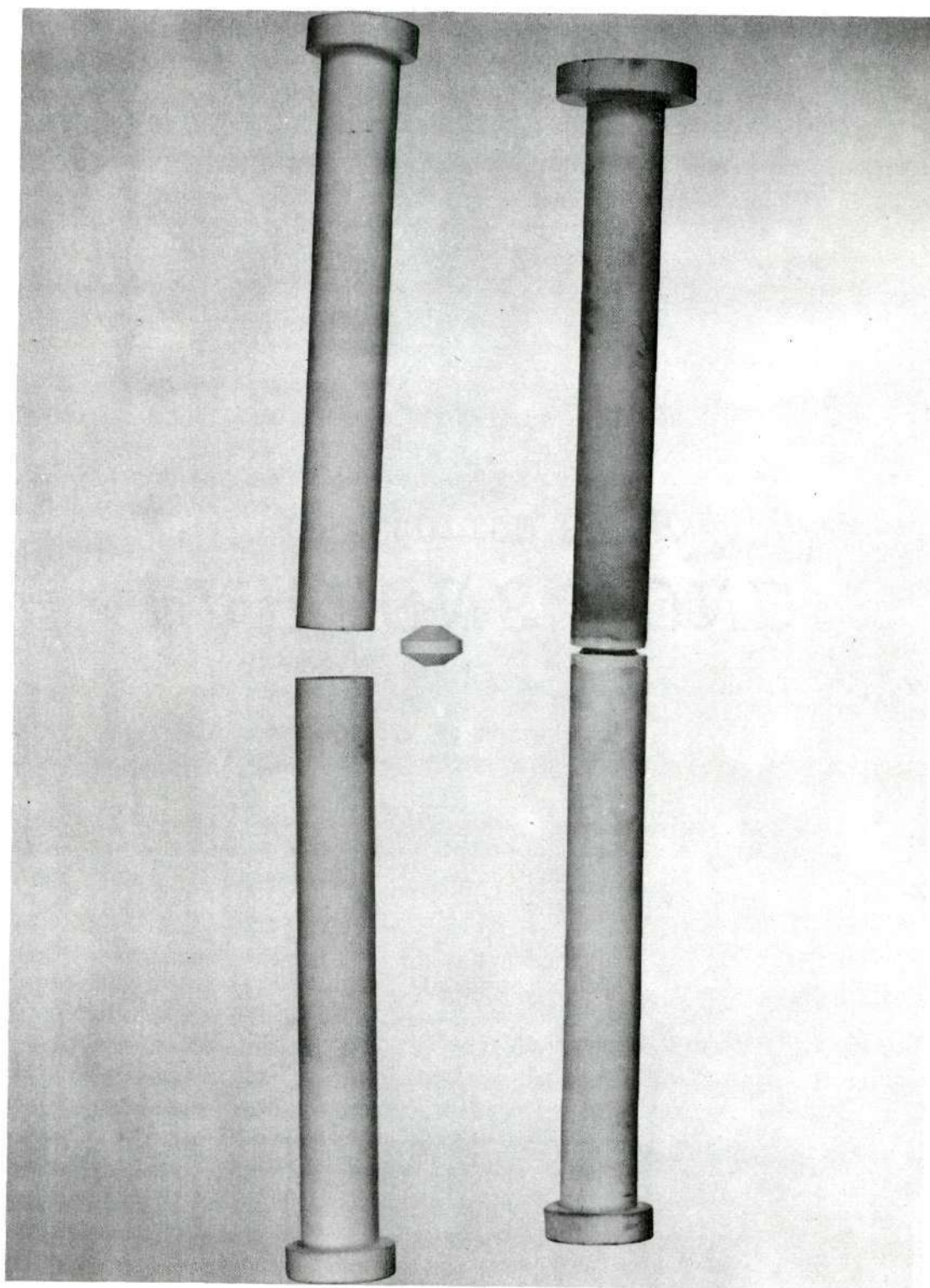


Figure 9. Assembled Test Specimens.

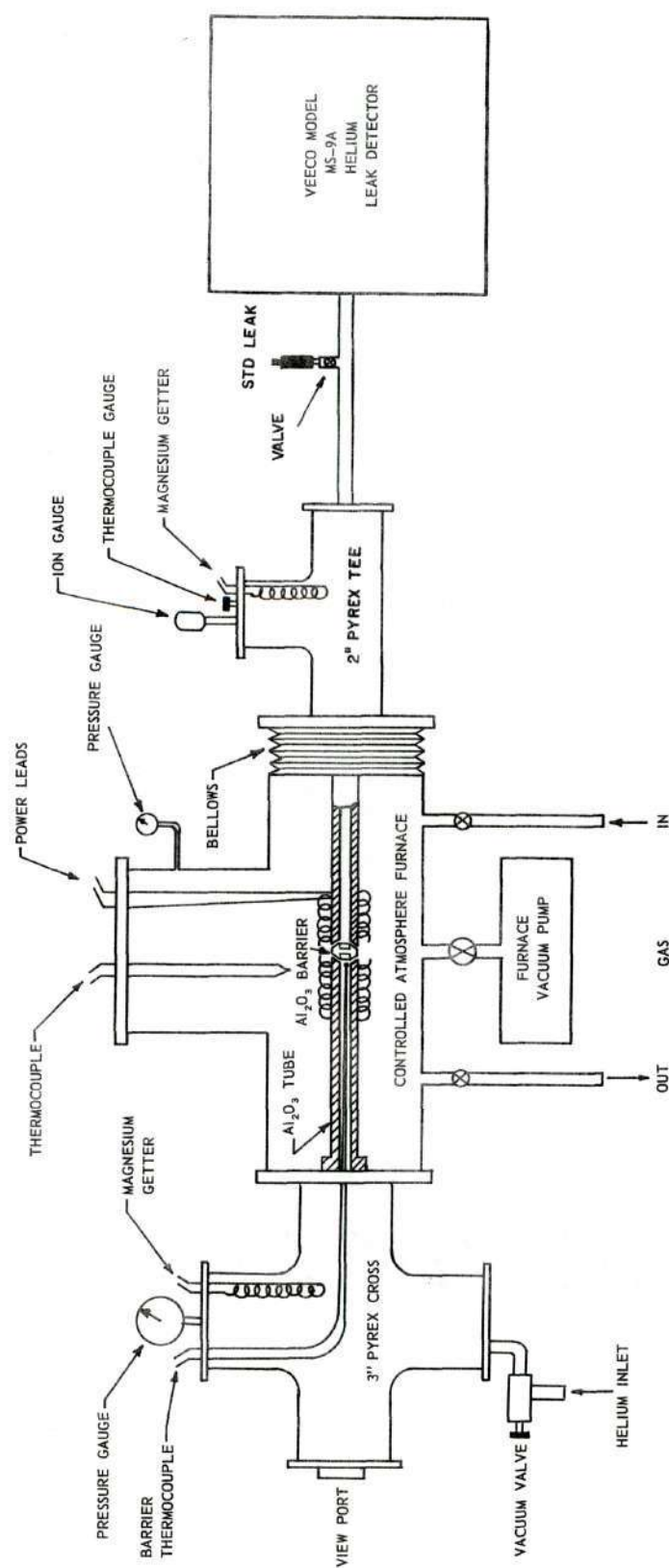


Figure 10. Diffusion Cell Schematic.

could be pumped down to the micron range, and it could be continually purged with a gas of zero helium content such as nitrogen.

The vacuum on the high vacuum side of the barrier was obtained from the pumping station included in the mass spectrometer unit. The station consisted of a mechanical pump, oil diffusion pump, and a cold trap charged with liquid nitrogen. Pressures inside the system were measured with a cold cathode discharge gauge located at the mass spectrometer tube, and an ion gauge and thermocouple gauge located at the end of the furnace assembly. The mass spectrometer was a standard Veeco model MS-9A helium Leak Detector. All permanent connections in the system were silver soldered, and critical "O" rings, not in the high vacuum assembly, were lubricated with Celvacene Heavy vacuum grease, supplied by the Consolidated Electrodynamics Corporation.

The barrier and tube assembly were surrounded by a Kanthal resistance heating element powered optionally by a saturable reactor and temperature controller, or by a powerstat. Thermocouples were placed at the barrier inside the assembly and at the exterior of the assembly at the barrier.

The entire system was checked for leaks after assembly with a helium leak detector and helium probe. Usually a minimum of three days was required to pump down and degas the system to operating pressures of about 10^{-5} mm. Hg.

The electrical stability of the system, including the heating element, recorders, and the mass spectrometer with its pumping station was maintained with Sola constant voltage transformers. The transformers

insured small variations in specimen temperature at all temperature levels and constant pumping speeds in the mass spectrometer unit. The apparent sensitivity of the instrument would have varied with the pumping rate of the station, had the pumping rate not been held constant. Sensitivity checks that did not vary beyond the limits of error set by the manufacturer as well as the constant temperature of the specimen confirmed the stability of the electrical system.

The base line of the system was established before helium gas was admitted. The base line represented the lower limits of the sensitivity of the mass spectrometer, and this was determined to be 3×10^9 atoms/sec. of helium passing into the mass spectrometer. The unit was calibrated with a model SC-4 Sensitivity Calibrator, Appendix A. Both sides of the barrier were at pressures of 10^{-5} mm. Hg when the base line of the instrument was established. Helium at one atmosphere was admitted to the high pressure side of the barrier and the high vacuum side of the system was continuously sampled with the mass spectrometer to determine the presence of any diffusion products. Records were made of the pressure on the high vacuum side of the barrier as well as the barrier temperature. The instrument was recalibrated twice a day during the duration of each run.

When a steady state had been reached between leak rate, temperature, and pressure, about seventy two hours, the system was considered to be at equilibrium; and a higher temperature level was sought. The sampling and recording procedure was followed as before. The temperature levels investigated were room temperature and one hundred degree centigrade intervals from 300°C to the operating limits of the furnace, about 1000°C.

After the helium reached a steady flow at each temperature level, it was removed to observe the helium flow rate decrease.

Mathematics of Molecular Flow

Molecular Effusion.--Equation (1) gives the flow rate of a gas through a hole in a thin plate of area A in atoms/sec. For a given gas at a constant temperature the flow rate is linearly proportional to the square of the radius of the hole, the effusion pressure and Avogadro's number. Flow rate is dependent upon the square root of the temperature, the square of the radius, and the effusion pressure for varying temperatures.

Molecular Streaming or Knudsen Flow.--Equation (2) is the general Knudsen equation. For a given gas, the flow rate is linearly proportional to the cube of the radius, the pressure differential from one end of the capillary to the other, the length of the capillary, the friction factor due to atoms rebounding from the walls of the capillary, and the square root of the temperature.

Poiseuille or Streamline Flow.--The standard form of Poiseuille's law is given by eq. (4). Correction factors may be applied to this equation as shown in the Survey of Literature according to Barrer. The application of these corrections results in eq. (7). This equation is identical to the Knudsen Equation except for numerical constants. Flow rate is linearly proportional to the pressure differential and to the other system constants.

Turbulent Flow.--The equation of flow for turbulent conditions is given by eq. (9). Mass velocity, or flow rate, is a complex function of the square root of the Reynolds number, fluid density, and hydraulic radius at a constant temperature.

Mathematics of Diffusion

A method of solving for the diffusion coefficient, D , and the activation energy for plane membrane diffusion is given by Barrer (34), Figure 11.

Fick's second law states:

$$\frac{\partial C}{\partial t} = D \frac{\partial^2 C}{\partial X^2} = 0 \quad (23)$$

for the steady state. The boundary conditions for a gas diffusing through a plate of thickness d are: $C = C_1$ at $X = 0$ for all time and $C = C_2$ at $X = d$ for all time. The term C represents the concentration of gas in atoms inside the plate anywhere from $X = 0$ to $X = d$.

The solution $C = AX + B$ of $D \frac{\partial^2 C}{\partial X^2} = 0$ for the steady state may be elucidated by inserting the boundary conditions $X = 0$ and $X = d$ and eliminating A and B . This leads to:

$$\frac{C - C_1}{C_2 - C_1} = \frac{X}{d} \quad (24)$$

where C_1 is the concentration of atoms/cm.³ at $X = 0$ and C_2 is the concentration in atoms/cm.³ at $X = d$.

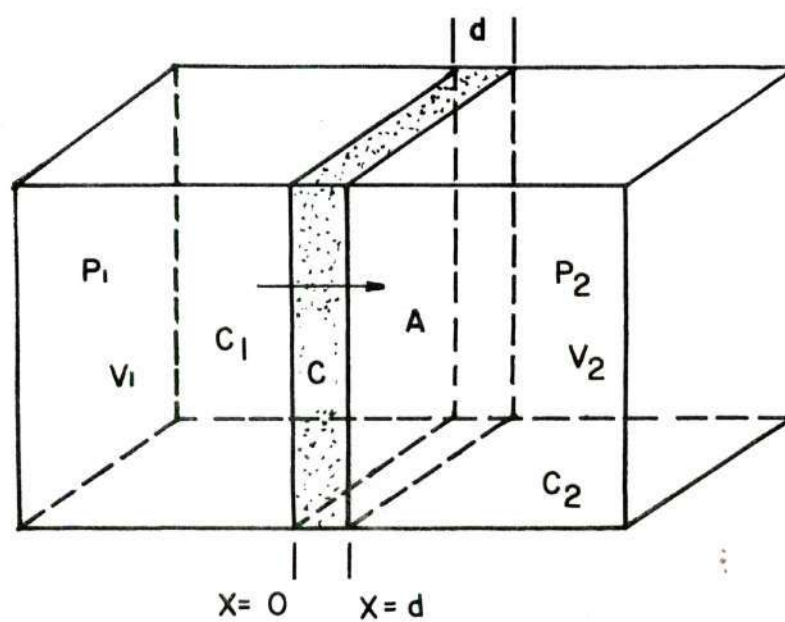


Figure 11. Plane Membrane Diffusion.

The total flow through a unit area of the plate is:

$$V \frac{dC_g}{dt} = - D \left. \frac{dc}{dx} \right]_{x=d} = D \frac{(c_1 - c_2)}{d} \quad (25)$$

where C_g = the concentration of gas in atoms/cm.³ which has diffused through the plate into the volume V at time t per unit plate area.

The condition that $C = C_2$ at $x = d$ for all t makes it necessary that $C_g \ll C_2$. Then the amount of gas which has diffused in time t is:

$$C_g = D \frac{(c_1 - c_2)}{dV_2} t \quad (26)$$

We may average eq. (26) and solve for D for a given plate area.

$$D = V_2 C_g \frac{d}{A} \frac{1}{(c_1 - c_2)} \frac{1}{t} \quad (27)$$

where $V_2 C_g$ = the total amount of atoms that have diffused in time t . This equals M .

c_1 = Concentration in atoms/cm.³ on the high pressure side of the barrier at $x = 0$

c_2 = Concentration in atoms/cm.³ on the low pressure side of the barrier at $x = d$.

d = The barrier thickness

A = The barrier area

t = The time for diffusion.

For the diffusion cell used in this work, eq. (27) may be further simplified. c_2 is much less than c_1 because of the low pressures associated with the high vacuum side of the system. This term may be neglected. Eq. (27) simplifies when diffusing into a unit volume V_2 to:

$$D = M \frac{d}{A} \frac{1}{c_1} \frac{1}{t} \quad (28)$$

where the units are the same as in eq. (27).

To determine the concentration c_1 on the high pressure side of the barrier we consider a unit volume V_1 at the barrier at temperature T_1 . From the perfect gas law, $PV = nRT$, we may solve for the concentration of gas in atoms in a unit volume, V_1 , at temperature, T_1 , with Arogadro's number.

Preparation of Electron Micrographs

Two specimens of alumina were selected for electron micrograph studies. A Carborundum Company alumina specimen was cut so that a cross-section of the barrier could be viewed. A Lucalox alumina specimen was examined on a surface face.

Both specimens were rough polished with a 100-mesh diamond lapping wheel for fifteen minutes. The final polish was accomplished by further lapping by standard techniques with 6μ diamond paste supplied by Buehler Ltd. The final polish lasted two to three hours. Examination of the surface with a 100x optical microscope determined the length of time of the final polish.

The specimens were etched for twenty minutes in hot (280°C) concentrated H_3PO_4 . The method is outlined by Scheuplein, et al. (35) and modified by Kriegel (36). The etch is a very slow one and there is very little danger of an over etch. For this work only one etching time was utilized, so no correlation was obtained between etching time and the amount of etching obtained. Visual examination under a 100x optical microscope with plain and oblique lighting showed no visible changes in the alumina surface at 5, 10, 15, and 20 minutes. During the etching period, the solution was continually stirred to prevent the formation of bubbles on the alumina surface. The etched samples were cleaned and dried.

Negative replicas were made of the areas of interest on both samples. The replicating material was PVA, applied by standard techniques. The negative replicas were chrome shadowed at 45°. The examination with the electron microscope was at 23,000x, including negative enlargement.

CHAPTER IV

DISCUSSION OF RESULTS

The physical dimensions of the specimens studied during the course of this investigation are listed in Table 6. Dimensions of samples that were obtained, but not examined for the diffusion constants in this work for various reasons, are listed in Table 7. Figures 12 through 17 graphically show the experimental data collected for specimens D through J. Table 8 lists the values of the diffusion constant at various temperature levels for each specimen, except G, which exhibited mass transport by a flow mechanism rather than a diffusion mechanism. Table 9 lists the experimentally determined values of the diffusion equation.

A plot of the \ln values of the coefficient of diffusion, D , approximate a straight line when plotted versus the reciprocal of temperature. The slope of the line was a function of the activation energy. Although a discontinuity in the diffusion coefficient occurred at elevated temperatures in series J, the values approximated separate straight lines with varies slopes above and below the inflection temperature as shown in Figure 18. The calculated activation energy, as calculated by Moody and Campbell (37), (38) and given in Appendix C and Figure 19, for interstitial diffusion of helium through the basal plane of Al_2O_3 was 5.7 ev while a value of 0.2 ev was determined for an edge dislocation activation energy.

Table 6. Physical Dimensions of Specimens

Specimen	Crystal Form	Barrier Thickness (cm)	Barrier Diameter (cm)	Pre-Test Thermal Treatment	Test Thermal Treatment	Density
D	Polycrystalline	0.149	0.635	Seal plus 2 firings	1 cycle	3.982
E	Polycrystalline	0.144	0.635	Seal plus 2 firings	1 cycle	3.972
F	Polycrystalline	0.076	0.635	Seal plus 2 firings	1 cycle	3.901
G	Polycrystalline	0.109	0.635	Seal plus 2 firings	1 cycle	---
H	Polycrystalline	0.107	0.635	Seal plus 21 firings	1 cycle	3.875
J	Polycrystalline	0.180	0.635	Seal plus 3 firings	1 cycle	3.703

Table 7. Physical Dimensions of Specimens Not Completely Studied

Specimen	Crystal Form	Barrier Thickness (cm)	Barrier Diameter (cm)	Pre-Test Thermal Treatment	Test Thermal Treatment	Density
K	Polycrystalline	0.0585	0.635	Barrier Cracked on Firing	---	3.97 <u>2</u>
L	Polycrystalline	0.150	0.635	Seal plus 7 Firings, Leaked	---	3.97 <u>1</u>
M	Polycrystalline	0.119	0.635	Seal plus 17 Firings. Specimen Leaked and Failed to Sinter at 1650°C	---	3.86 <u>0</u>
N	Polycrystalline	0.158	0.635	Seal plus 2 Firings. Specimen Leaked and Failed to Sinter at 1650°C	---	3.77 <u>2</u>
O	Polycrystalline	0.140	0.635	Seal plus 3 Firings. Failed to Sinter at 1650°C	---	3.81 <u>1</u>
P	Polycrystalline	0.147	0.635	Seal plus 8 Firings. Failed to Match Seal to Body	---	3.85 <u>1</u>

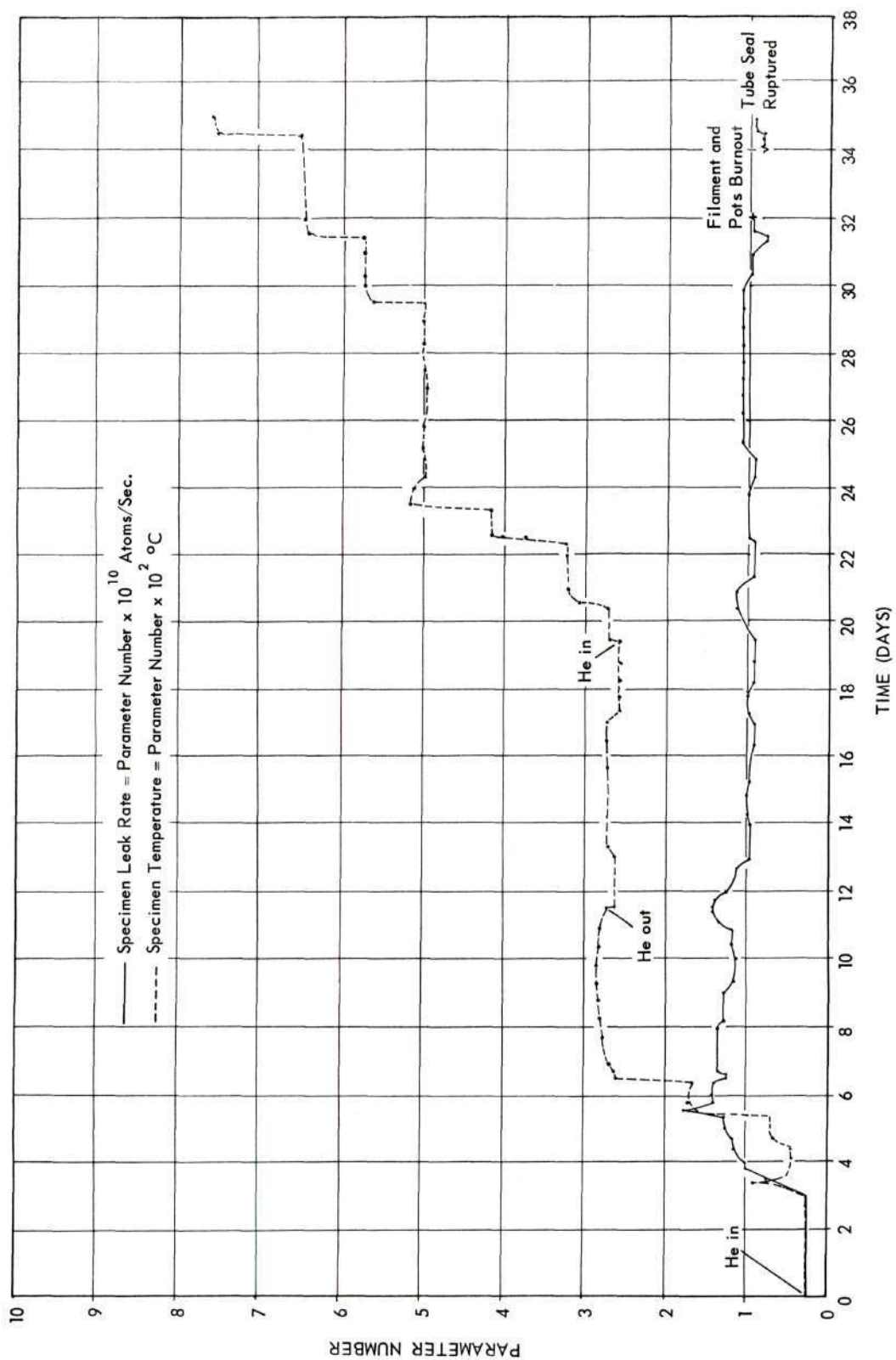


Figure 12. Average Data, Specimen D (see Appendix D).

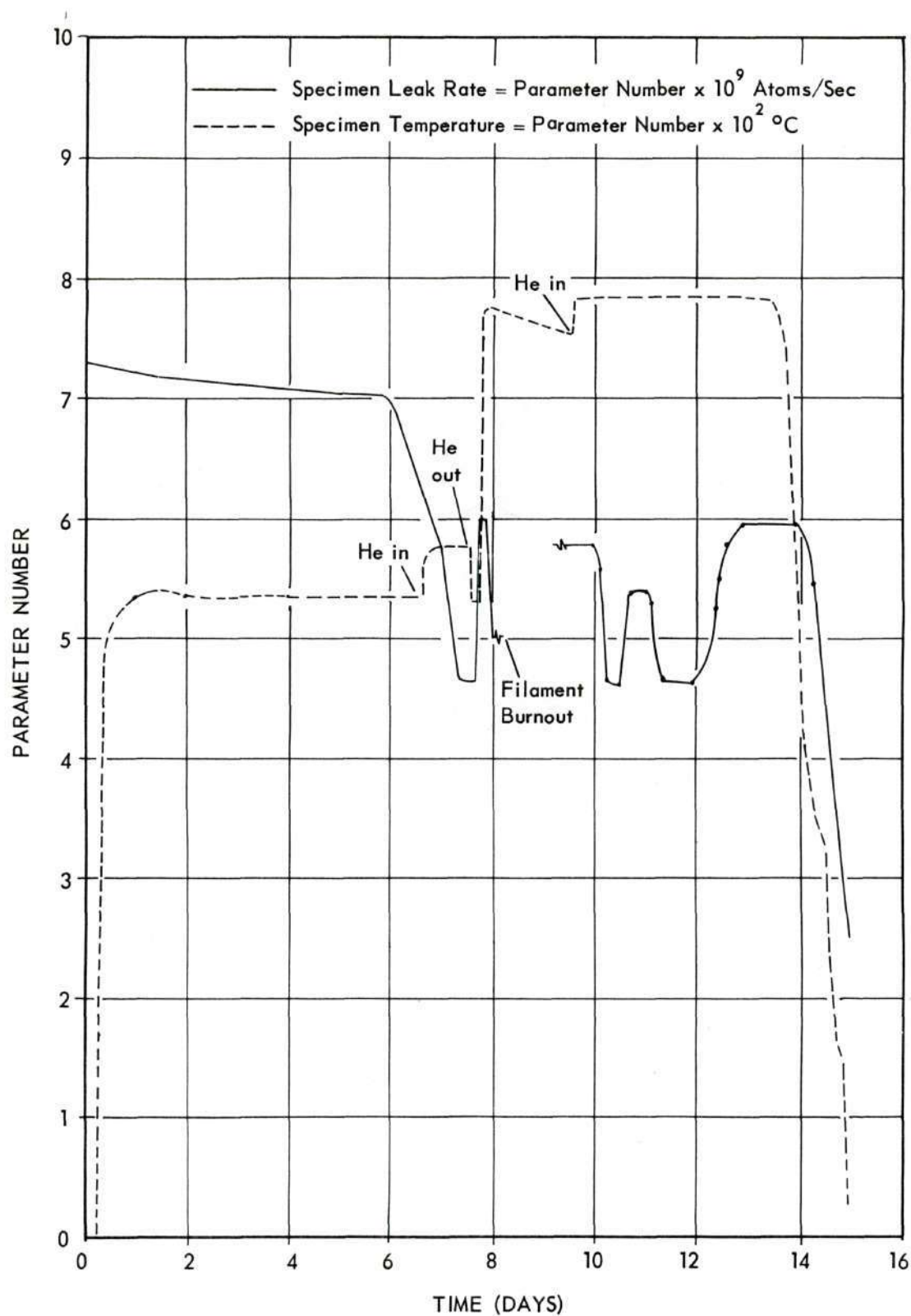


Figure 13. Average Data, Specimen E (see Appendix D).

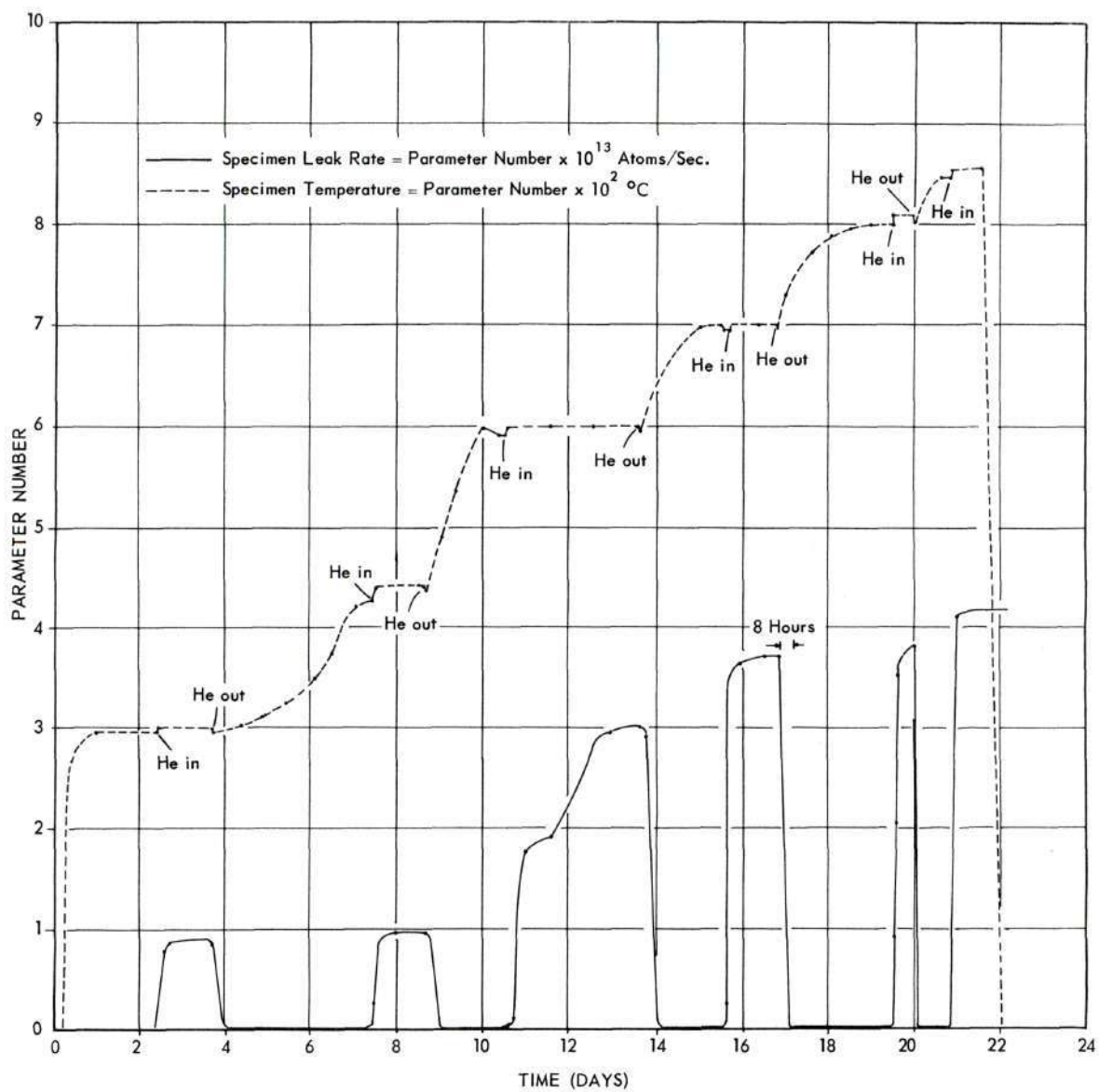


Figure 14. Average Data, Specimen F (see Appendix D).

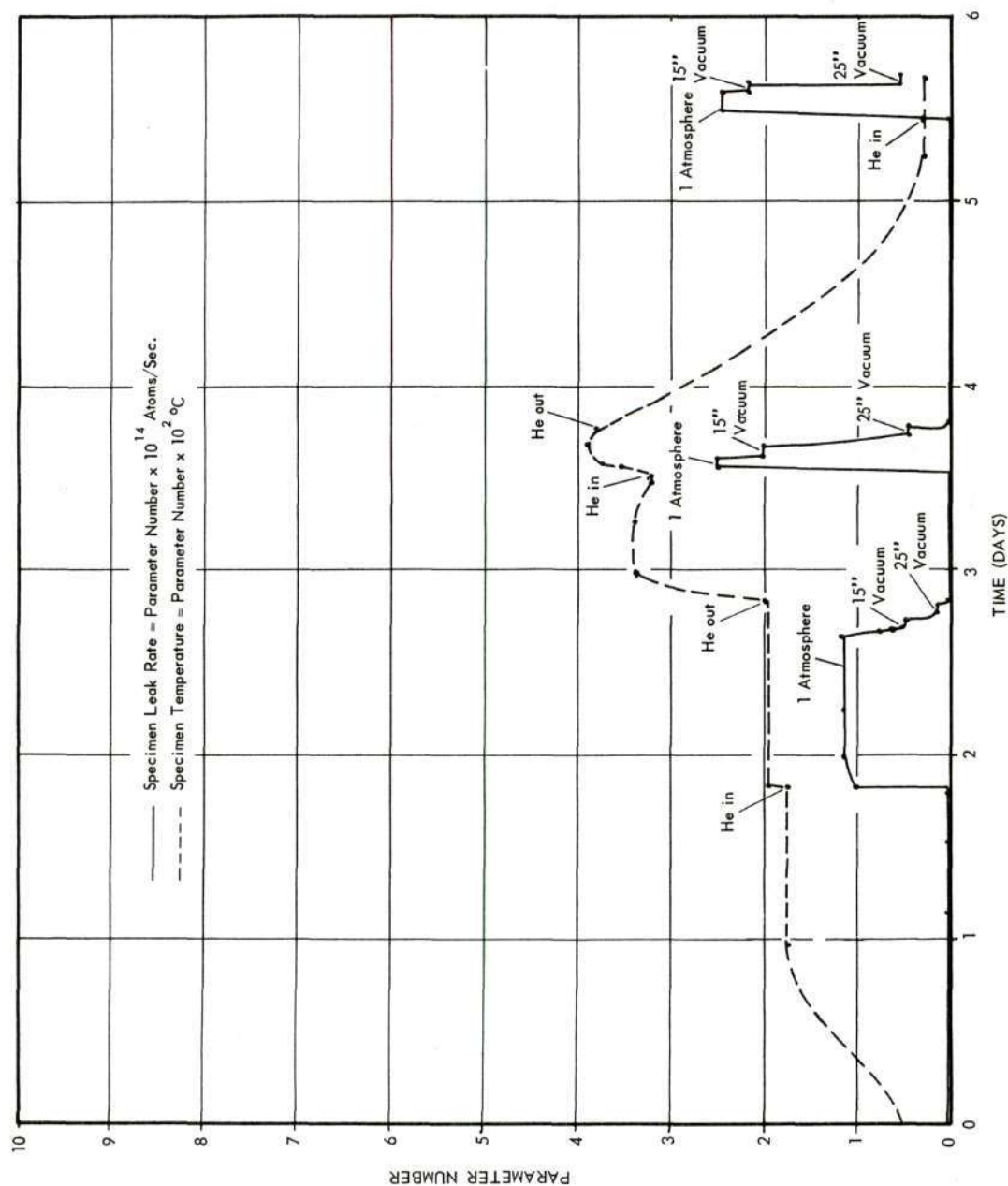


Figure 15. Average Data, Specimen G (see Appendix D).

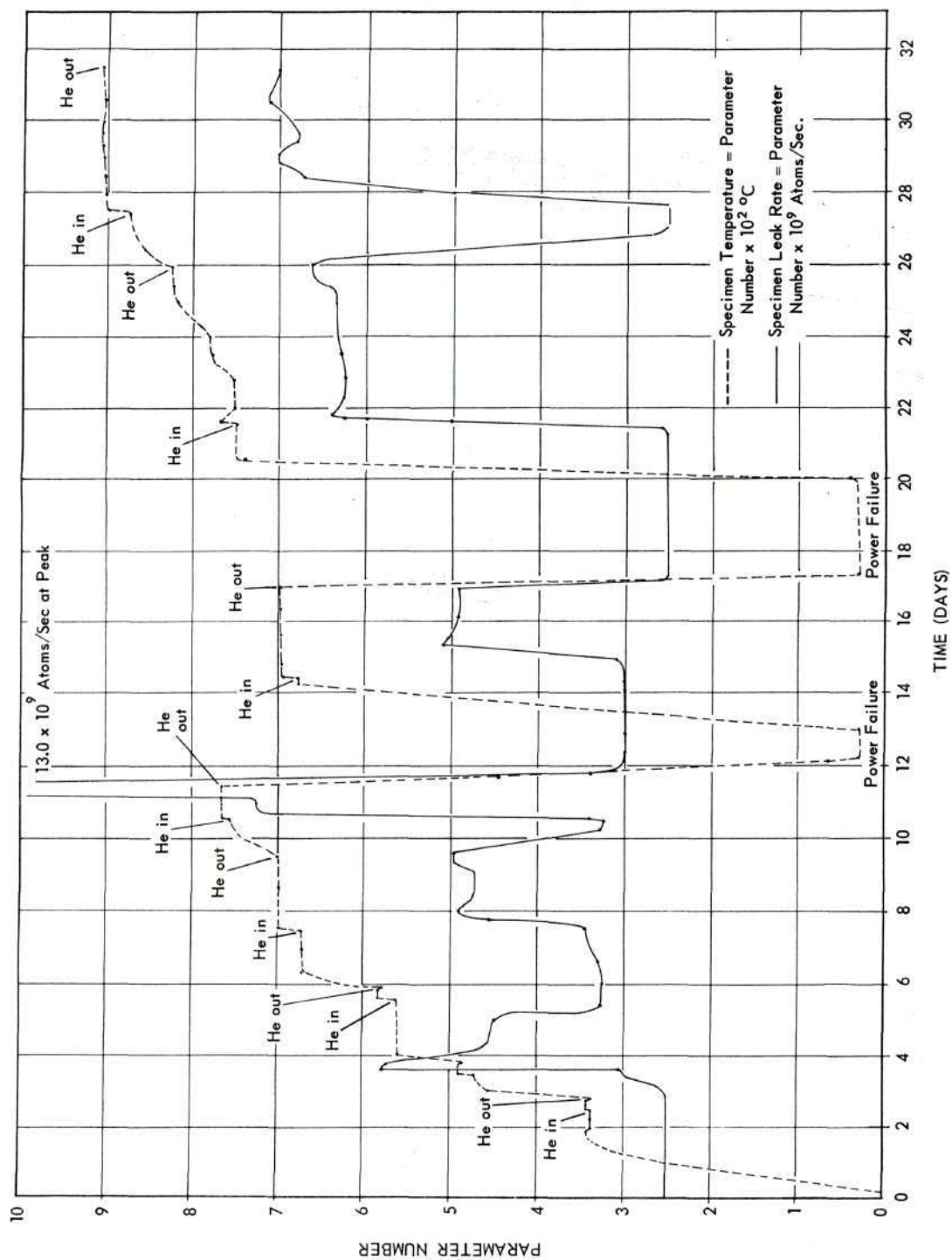


Figure 16. Average Data, Specimen H (see Appendix D).

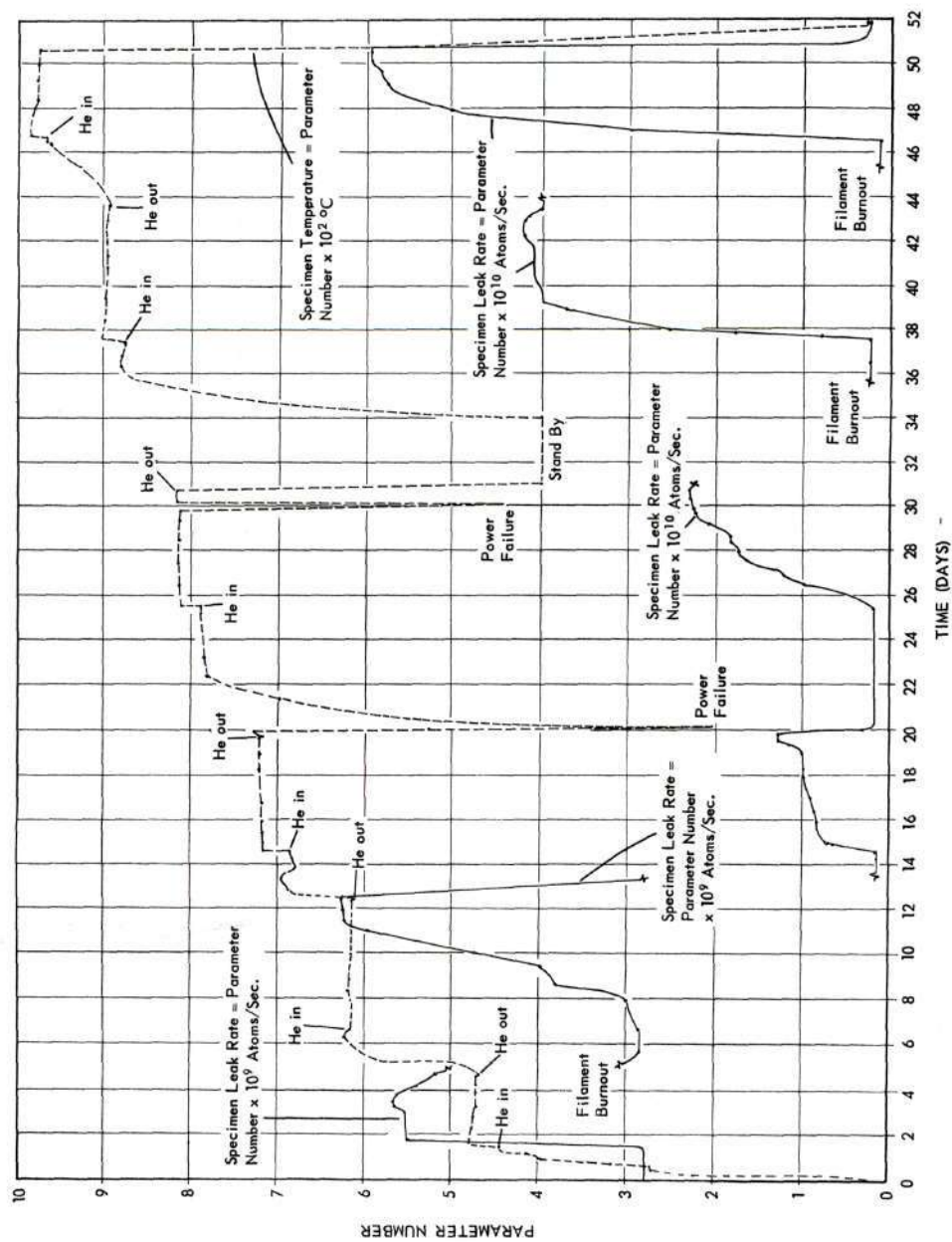


Figure 17. Average Data, Specimen J (see Appendix D).

Table 8. Diffusion Data

Specimen	Temperature	Diffusion Coefficient cm. ² sec. ⁻¹	$\frac{1}{T^{\circ}K} \times 10^3$
D	275	4.19×10^{-10}	1.825
	270	3.30×10^{-10}	1.84
	322	2.46×10^{-10}	1.68
	500	4.69×10^{-10}	1.30
	650	3.52×10^{-10}	1.08
	755	4.37×10^{-10}	0.98
E	790	1.98×10^{-10}	0.94
F	300	1.65×10^{-8}	1.75
	490	3.72×10^{-7}	1.32
	600	8.68×10^{-7}	1.15
	700	1.15×10^{-6}	1.02
	810	1.40×10^{-6}	0.92
	855	1.50×10^{-6}	0.90
G	---	---	---
H	705	8.54×10^{-11}	1.01
	782	1.50×10^{-10}	0.95
	825	1.72×10^{-10}	0.91
	902	2.18×10^{-10}	0.85

Table 8 (Continued)

Specimen	Temperature	Diffusion Coefficient $\text{cm.}^2 \text{sec.}^{-1}$	$\frac{1}{T^{\circ}\text{K}} \times 10^3$
J	475	1.68×10^{-10}	1.34
	615	2.39×10^{-10}	1.13
	722	7.80×10^{-10}	1.00
	812	1.72×10^{-9}	0.92
	896	3.54×10^{-9}	0.85
	975	5.50×10^{-9}	0.80

* Not true diffusion

Table 9. Experimental Values of the Diffusion Equation

Series	$D = D_0 \exp(-E_a/kT)$
D	Not determined
E	Not determined
F	$D = 1.52 \times 10^{-5} \exp(-0.222 \text{ ev}/kT)$
G	Exhibited laminar and turbulent flow
H	$D = 1.34 \times 10^{-8} \exp(-0.413 \text{ ev}/kT)$
J	$D = 1.26 \times 10^{-5} \exp(-0.830 \text{ ev}/kT)$

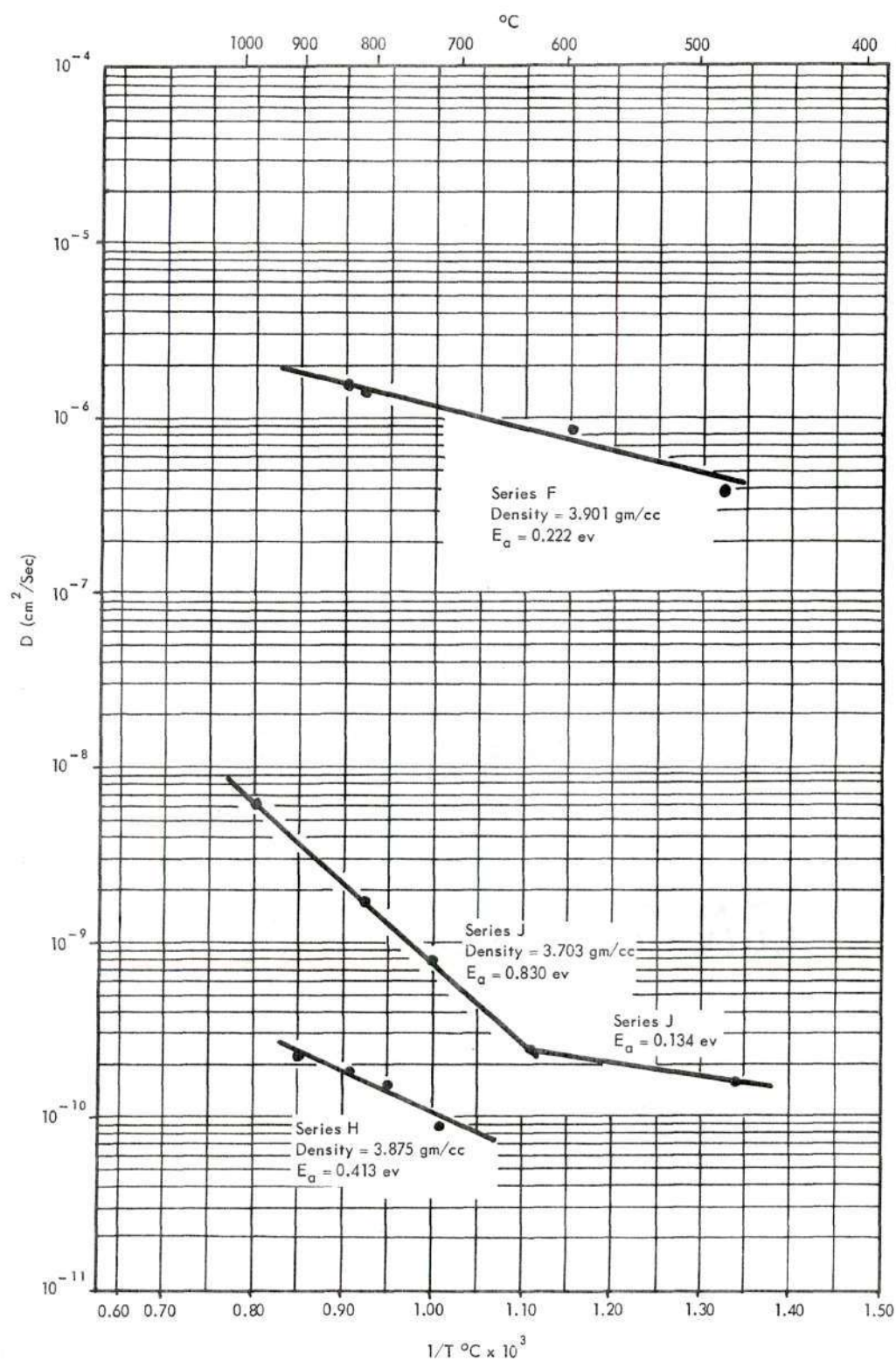


Figure 18. Helium Diffusion in Alumina.

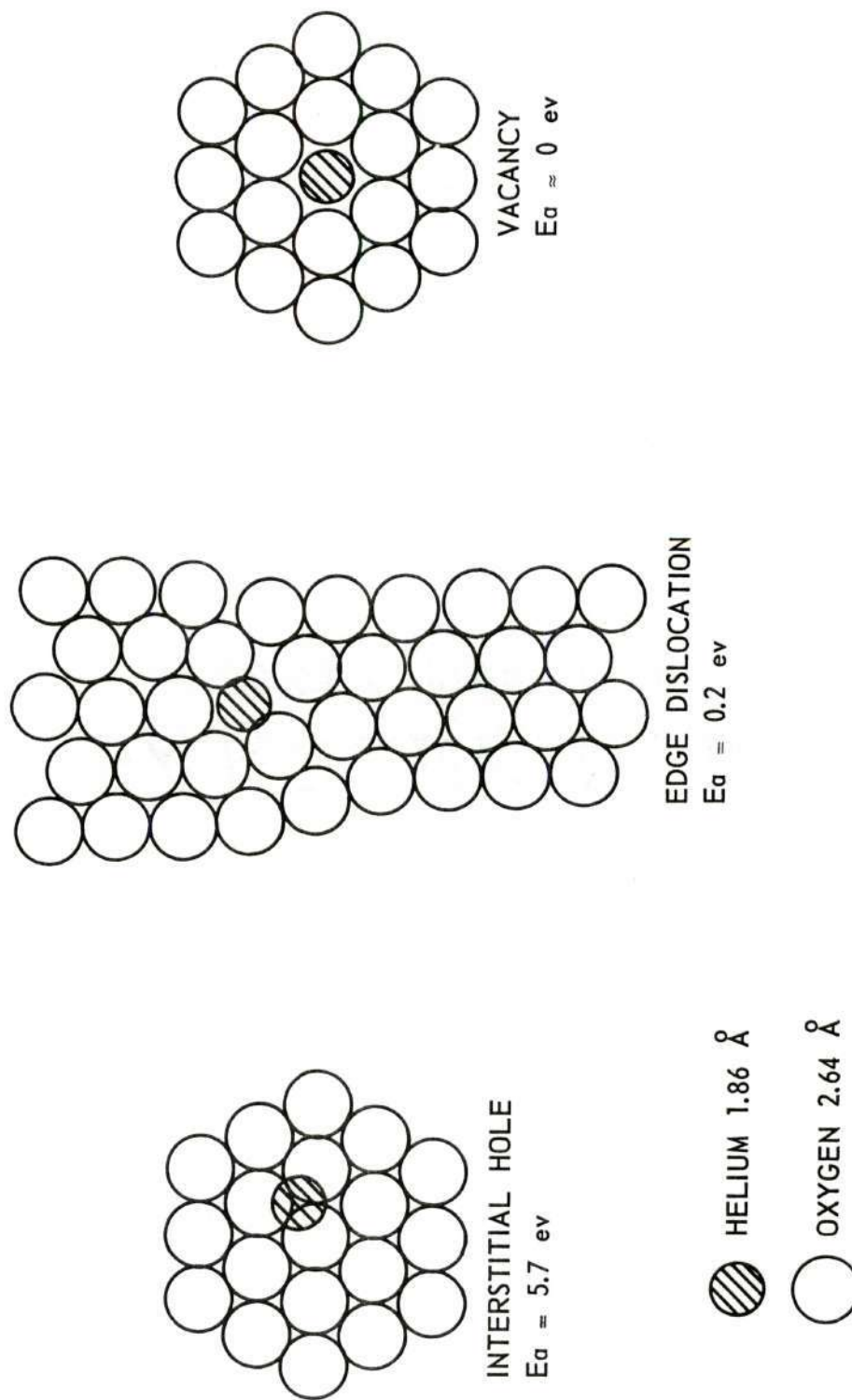


Figure 19. Calculated Activation Energies.

The path traversed by the helium atom in diffusion was considered as being between the barrier surfaces for the calculation of the coefficient of diffusion and diffusion constant, Appendix B. Measured values of the diffusion constant, D_0 , ranged from 10^{-8} cm.²/sec. to 10^{-6} cm.²/sec. The value of D_0 is a function of the number of short circuit diffusion paths present in a polycrystalline specimen. Campbell (39) reported values for D_0 of 10^{-8} cm.²/sec to 10^{-5} cm.²/sec. in the temperature range 25°C to 900°C. Linder (40) reported D_0 as 10^{-5} cm.²/sec. from 27°C to 150°C with a 92% alumina body. Generally, the lower the value of D_0 , when accompanied by low values of D , the greater is the importance of grain boundary or short circuit paths for diffusion.

Lucalox Alumina.--The time-temperature dependence of the flow of helium through two specimens of Lucalox Alumina is shown in Figures 12 and 13. No specimen leak rate rise above the base line was indicated up to 780°C as the rate could not be definitely interpreted analytically as the presence of diffusion products in either specimen. The x-ray density of single crystal alpha-alumina is 3.98 gm./cm.³, and the measured bulk density of the Lucalox specimens averaged 3.975 gm./cm.³. Since the Lucalox alumina had been treated with small amounts of MgO to aid in sintering and densification, it is quite possible that the Mg^{++} ions occupy some of the vacant sites in the alumina lattice as well as the grain boundary area. These additional ions quite probably had a marked effect on the diffusion mechanism.

Carborundum Company Alumina.--Figures 14, 15, 16, and 17 show the time-temperature dependence of the flow of helium through Carborundum Company alumina. Figure 16 is a special case and will be discussed subsequently. Figure 18 shows the results of plotting measured values of D versus the reciprocal temperature. Specimens F and H yield activation energy values of 0.222 ev. and 0.413 ev. respectively. Series H gives a calculated value of the diffusion constant, D_0 , of $1.34 \times 10^{-8} \text{ cm.}^2/\text{sec.}$, the lowest values measured in this series of experiments. This specimen gave values of the diffusion coefficient in the range of $10^{-10} \text{ cm.}^2/\text{sec.}$ Specimen F yielded values of the diffusion constant in the range of $10^{-6} \text{ cm.}^2/\text{sec.}$ The diffusion path of specimen H was one and four-tenths times as long as specimen F. The measured bulk densities varied within $\pm 0.026 \text{ gm./cm.}^3$, or $\pm 0.51\%$.

Figure 17 shows the time-temperature dependence of the flow of helium through specimen J. Appendix B, Table 10, shows a sample of the data collected during the course of this particular investigation as well as sample calculations. Specimen J had a barrier thickness 2.4 times as great as specimen F. The measured bulk density was five per cent lower. The calculated activation energy for specimen J was 0.830 ev., after the inflection point. The calculated activation energy of specimen J was approximately three and three-quarters times as high as for the specimen F. The value of the diffusion constant, D_0 , for both specimens was $1.40 \pm 0.10 \times 10^{-5} \text{ cm.}^2/\text{sec.}$ The relative importance of short circuit diffusion paths seems approximately the same.

Four points must be kept in mind when considering the experimentally calculated values of the activation energy.

The steady state leak rate readings at lower temperatures, below 500°C, during the early portions of the experiment must be subject to doubt. Figure 16, the data presentation for specimen H, shows that on the third day helium was admitted to the system with no rise in leak rate. The helium was then pumped out. The temperature was increased with no helium in the system, and the leak rate rose. The leak rate subsequently fell indicating that the contamination had finally been removed. Longer periods of time would have to be spent at lower temperatures to determine the magnitude of the true steady state.

The thickness of the barrier played an important role in the consideration of the next three points. If the barrier length is quite short, it is possible that only one grain occupies the entire length of the barrier. The single continuous grain boundary would provide an easy diffusion path, and a low activation energy would be expected. If the path were longer the diffusing atoms would have to follow several grain boundaries. Where one boundary terminated the diffusing atoms would have to search for another path to reach the next grain boundary. A mechanism of this type would require more energy than simple grain boundary diffusion. The longer path length would also require a longer time to reach the equilibrium state. This would be especially true at lower temperatures. Experimentally determined values of the steady state readings would be uniformly low if insufficient time were spent at an equilibrium temperature level.

Barriers were formed by ultrasonic impact grinding. If a barrier were formed of a thickness such that only one or two grains occupied the path length, it is possible that the entire barrier could be mechanically shocked in the formation operation, opening new diffusion paths.

Figure 15 shows the time-temperature dependence of the flow of helium through specimen G. This specimen was different for several reasons. The specimen leak rates recorded were five hundred to one thousand times greater than any experienced on the other five specimens studied. The time necessary to reach an equilibrium flow rate was never in excess of ten to fifteen minutes. The specimen leak rate was temperature dependent and highly pressure dependent during the heating cycle. The specimen leak rate after cycling from 400°C to room temperature had changed and was higher than at 400°C. Specimen leak rate was still pressure dependent. The higher leak rate after the heating cycle indicated that structural damage was done to the material. The types of molecular flow processes mentioned earlier were considered in order to determine, if possible, the type of flow that this specimen exhibited.

A plot was made of dn/dt , the equilibrium flow rate in atoms/sec. as a function of the pressure differential across the length of the barrier at a constant temperature, Figure 20. The equations for laminar flow, eq. (1) through (7), all state that the flow rate at a constant temperature is linearly proportional to the pressure differential. The pressure on the high vacuum side of the barrier was less than 10^{-5} mm. Hg and may be neglected. Any deviation from a linear function at different temperature levels would indicate a divergence from laminar flow.

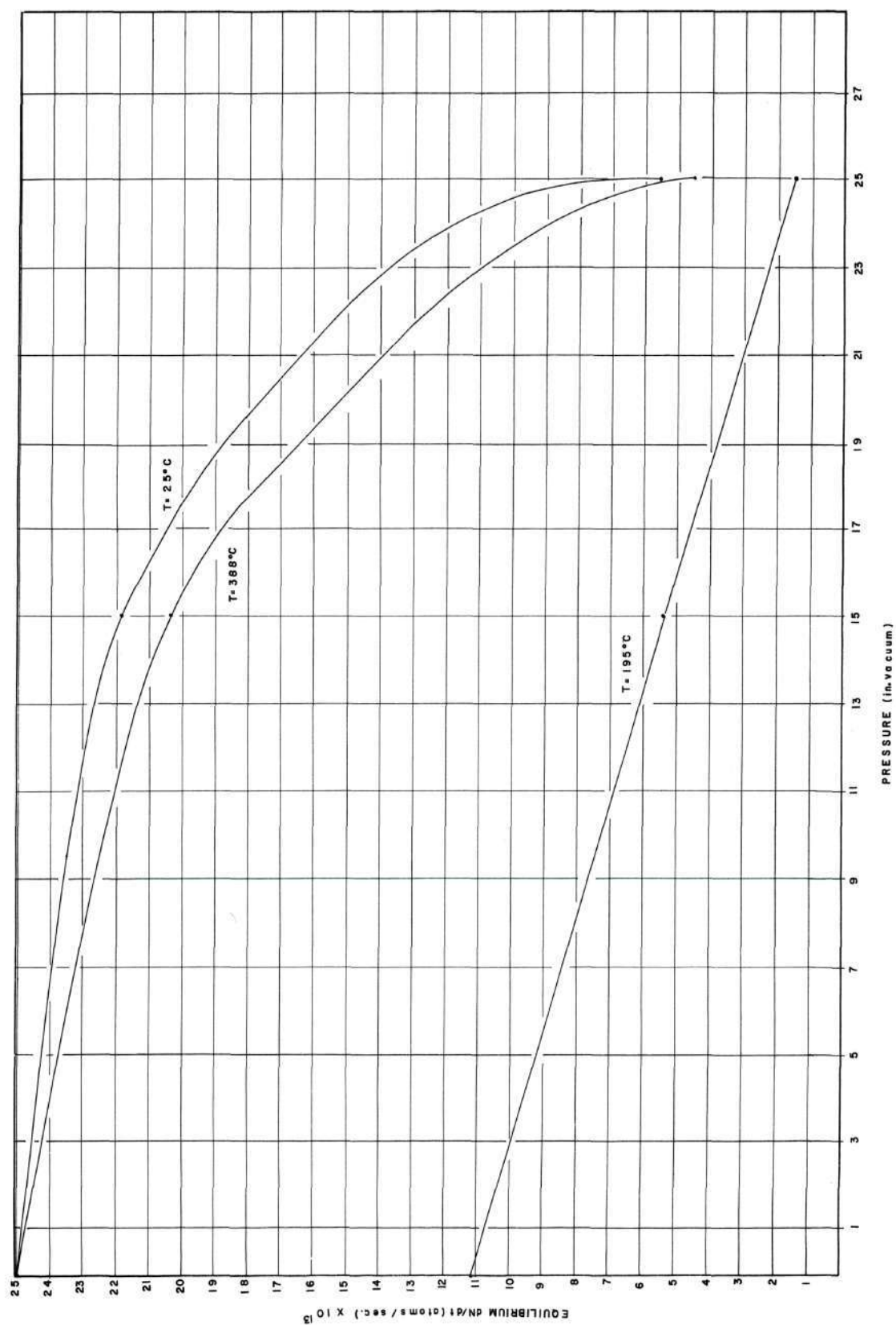


Figure 20. Equilibrium Flow Rates, Specimen G.

Figure 20 shows that during the heating cycle at 195°C , the measured values approximate a straight line very closely. The flow is apparently laminar. At 383°C , the next temperature level, the same type of plot deviates from a straight line, and the flow rate increased. This is apparently a turbulent flow. The system was then cooled down to room temperature and helium was admitted to the system. The room temperature leak rates recorded were higher than at 383°C indicating that still further damage had been done to the specimen. The plot deviated from a straight line indicating a turbulent flow as the helium passed down the path. The type of flow experienced at 195°C can be predicted to some extent. The flow could not have been molecular effusion through an orifice since the gas did have a finite distance to travel. This leaves no molecular streaming (Knudsen flow) or Poiseuille types of flow. These types of flow are both linearly dependent upon pressure differential. Since nothing is known about the coefficient of slippage on the wall or the value of the radius of the hole in the specimen there is no method of separating one type of flow from the other. The only conclusion that can be drawn is that at 195°C , the flow was not turbulent.

One further point should be noted. The time necessary to reach equilibrium conditions on flow rate for specimen G was approximately ten minutes. Specimens F, H, and J all required a minimum of eight hours to come to equilibrium. Specimen J, the thickest specimen studied, did not reach equilibrium conditions in less than three days at the temperature levels studied, see Figure 17. Since the barrier thickness of specimen G and specimen H were practically the same and the barrier thickness of

specimen F was even thinner, the length of time necessary to reach steady state flow rate is a strong argument for the diffusion mechanism of atomic mass transport.

Electron Micrograph Studies of Alumina.--Electron micrographs of two samples of alumina are shown in Figures 21, 22, 23, and 24. The Carborundum Company alumina sample exhibited a grey-white area to either side of the barrier area due to carbon pick-up in the formation process. An electron micrograph was made of this area to determine if there were any structural differences peculiar to the area.

Figure 21 is an electron micrograph of a sample of Lucalox alumina, specimen D. One grain appears to occupy the major portion of the field, and there are several lines that may be microcracks in the interior of the grain. Generally, the area seems to be free from an excessive number of defects. The dark spots that occur randomly in the field are particles of polishing grit, six micron diamond.

Figures 22, 23, and 24 are micrographs of a sample of Carborundum Company alumina. No diffusion studies had been made on this sample. The sample had been fired to 1650°C after the barrier had been formed. The figures represent different areas of the sample surface. Figure 22 was taken from the middle of the cross-section of the barrier area. The microstructure appears to be very fine. The only prominent area in the field is what appears to be a grain boundary running from the upper left to the lower right of the micrograph. Surface microcracks appear to radiate out along the grain boundary. The lower left corner of the

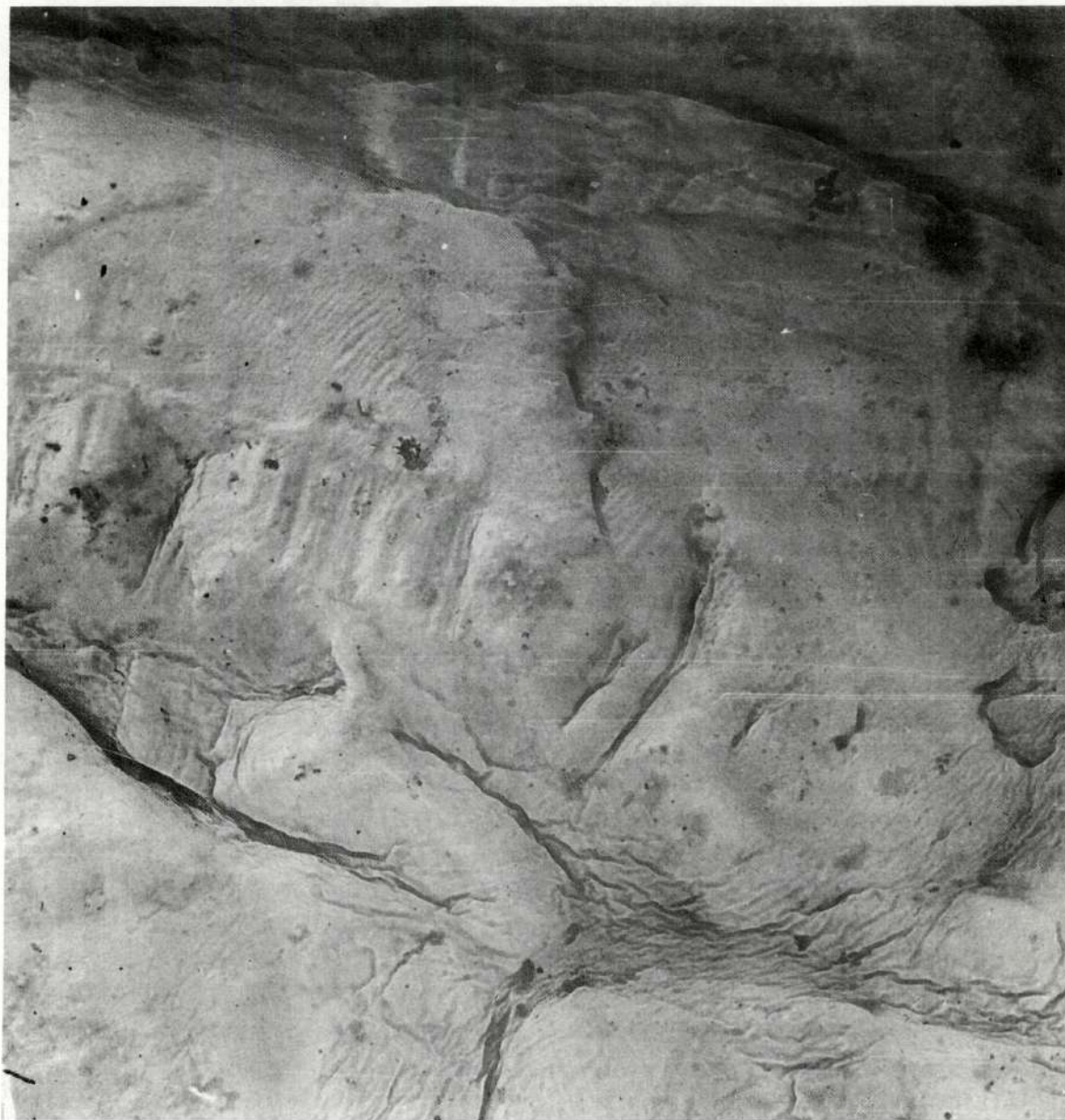


Figure 21. Electron Micrograph of Lucalox Alumina. (One grain occupies the major portion of the field. Note the absence of lines and voids in this material (22,400X).)

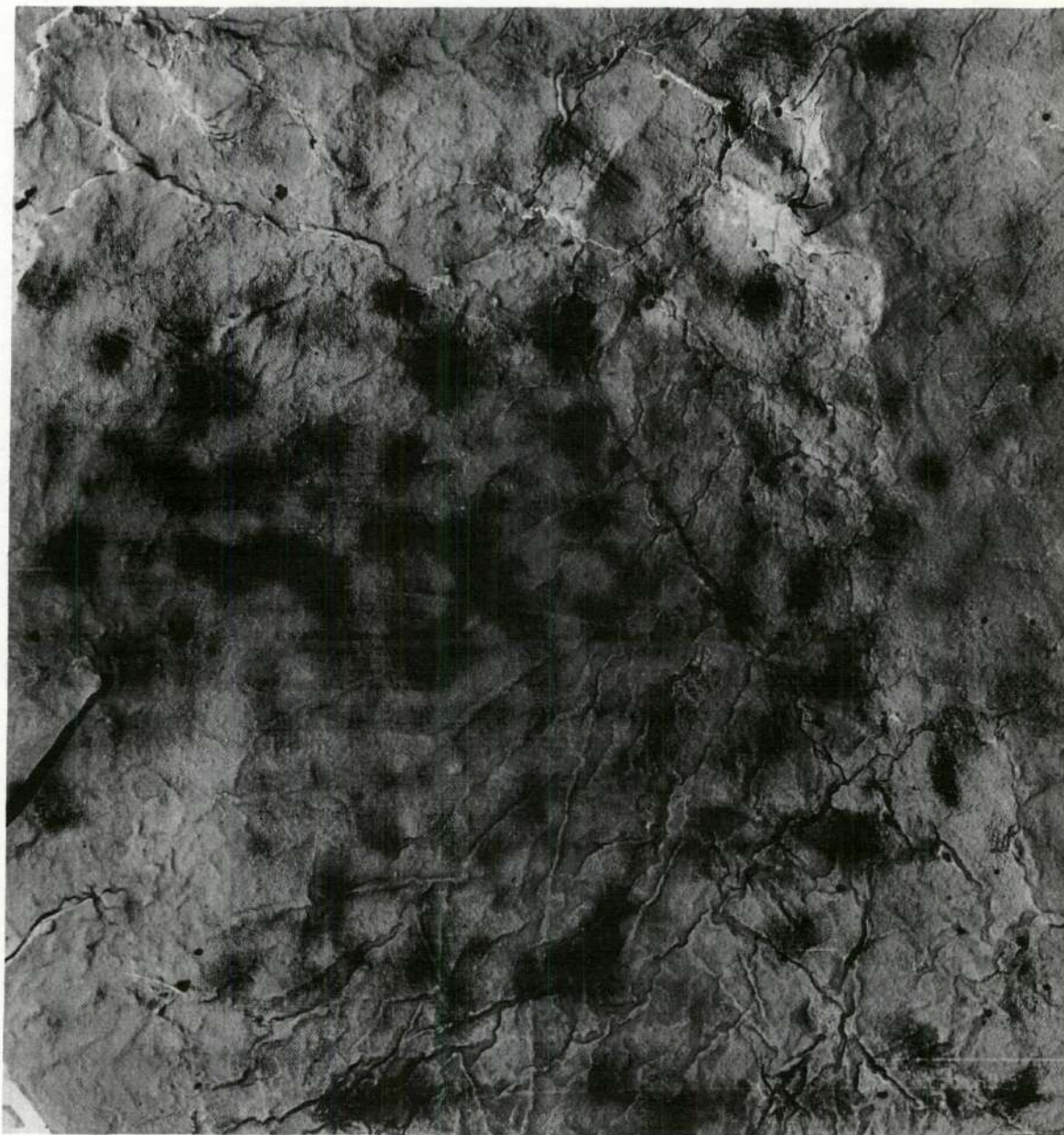


Figure 22. Electron Micrograph of a Carborundum Co. Polycrystalline Alumina Sample. (A grain may be seen in the upper right. Lines that may be microcracks appear over the entire field. Dark areas are polishing grit (22,700X).)



Figure 23. Electron Micrograph of the Area to One Side of the Barrier of a Carborundum Co. Polycrystalline Alumina Sample. (What appear to be microcracks radiate from the depression at the lower right (23,000X).)



Figure 24. Electron Micrograph of the Outer Area of a Carborundum Co. Polycrystalline Alumina Sample. (Large numbers of microcracks radiate at random over the entire field (23,000X).)

micrograph shows a triangular surface that slopes down and away from the surface of the replica. This sloping surface could indicate a fracture or parting in one grain. Dark spots on the surface are the results of polishing grit.

Figure 23 is a micrograph of the area of carbon pick-up located to either side of the barrier cross-section. The most noticeable feature in the micrograph is the large depression that appears in the lower right hand corner. Since the micrograph shows a negative replica of the sample, what appears as high points in the micrograph are depressions in the original sample. There appears to be no difference in the structure of the material in the interior of the depression. The depression could have been present at the time the specimen was hot pressed, or it could have been produced during the polishing operation. The stresses that accompanied the cutting and polishing operations could have been sufficient to tear a weakly bonded grain out of the matrix of the structure. There appear to be more lines that could be microcracks in this area than were present in the micrograph of the barrier cross-section.

Figure 24 is a micrograph of the outer edge of the sample. The prominent feature is a large depression. There appear to be many more microcracks in this area than were present in Figures 22 and 23.

Figures 22, 23, and 24 were all taken from the same specimen. The number of lines that appear to be microcracks increases from the barrier area into the interior of the sample. The barrier area would always receive an even heating due to its relatively thin cross-section. Heat conduction becomes much more complicated in the interior of the sample

which has a much greater mass. This could account for the lines that might be microcracks; since non-uniform heating produces stresses.

Examination of Figures 21 and 22 shows that the Lucalox sample has fewer lines than does the Carborundum Company alumina. These could be surface cracks that might be entrances to diffusion paths in the interior of the sample.

CHAPTER V

CONCLUSIONS

1. Two Lucalox alumina specimens exhibited helium diffusion rates below the sensitivity of the helium mass spectrometer in the temperature range 25°C to 900°C. This indicates diffusion coefficients smaller than 10^{-11} cm.²/sec.

2. The Carborundum Company alumina samples yielded values of the diffusion coefficient ranging from 10^{-11} cm.²/sec. to 10^{-6} cm.²/sec. and activation energy values of 0.222 ev., 0.412 ev., and 0.830 ev. for series F, H, and J, respectively.

3. Series J exhibited a discontinuity temperature at which the experimentally determined value of the activation energy took a new higher value. This might have been caused by the annealing out of dislocations in the basal plane of the Al_2O_3 lattice.

4. Electron micrograph studies show that the Lucalox alumina has a surface much more free from lines than does the Carborundum Company alumina. These lines appear to be microcracks.

5. These lines in the surface of the Carborundum Company alumina that might be microcracks could be the entrances to interior diffusing paths for the helium gas.

6. For the Carborundum Company alumina samples studied, the values of the activation energy indicate that the diffusion process might be an atom vacancy type along grain boundaries with small amounts of interstitial diffusion.

7. The activation energy seemed to increase with increased barrier thickness for small density variations of $3.85 \pm 5\%$ gm./cc.

BIBLIOGRAPHY

1. Flint, P. S., The Diffusion of Hydrogen through Materials of Construction, KAPL - 659, Knolls Atomic Powder Laboratory, 1951, p. 9.
2. Ibid., p. 9.
3. Handbook of Chemistry and Physics, Hodgman, C. D., 41st Edition, Chemical Rubber Publishing Co., 1960, p. 3089.
4. Kirkland, C. G., Determining Trace Impurities in Grade-A Helium, RI-5644, Bureau of Mines, United States Department of the Interior, 1960.
5. Wyckoff, R. W. G., Crystal Structures, 2, 5, Interscience Publishers, 1951, text page 4, illustration page 3.
6. Krunberg, M. L., "Plastic Deformation of Sapphire," Acta Metallurgica, 5, 1957, pp. 507-511.
7. Wells, A. F., Structural Inorganic Chemistry, Oxford University Press, 1950, pp. 364-389.
8. Wyckoff, op. cit., p. 4.
9. Ibid., p. 4.
10. Krunberg, op. cit., p. 508.
11. Ibid., p. 508.
12. Russell, A. S., Alumina Properties, Technical Paper No. 10 (revised), Alcoa, 1956, 10 pp.
13. Klein, D. S., Measurement of the Crystallographic Thermal Expansion of Alpha-Alumina and Beryllia to Elevated Temperatures Emphasizing Anisotropic Effects, National Aeronautical Administration, NAA-SR-2542, 1958, 24 pp.
14. Sinnott, M. J., The Solid State for Engineers, John Wiley and Sons, 1958, pp. 253-276.
15. Seitz, F., The Modern Theory of Solids, McGraw Hill, 1940, pp. 494-499, 548-558.
16. Baumann, H. N., "Crystal Habits of Alpha-Alumina in Alumina Ceramics," Bulletin of the American Ceramic Society, 37, 4, pp. 179-184, 1958.

17. Sinnott, op. cit., pp. 253-276.
18. Klein, op. cit., pp. 1-24.
19. Barrer, R. M., Diffusion in and through Solids, Cambridge University Press, 1941, Chapter II.
20. Ibid., pp. 53-58.
21. Klose, Von Wilhelm, "Über die Stromung verdünnter Gase durch Kapillaren," Annalen der Physik, Leipzig, 11, series 5, pp. 73-79, 1931.
22. Seitz, F., "Fundamentals of Diffusion in Solids," Phase Transformations in Solids, Smoluchowski, R., Symposium at Cornell University, John Wiley and Sons, 1948, pp. 77-149.
23. Seitz, "Fundamentals of Diffusion in Solids," op. cit., p. 80.
24. Barrer, op. cit., pp. 1-51.
25. Zener, C., "Theory of D_0 for Diffusion in Metals," Journal of Applied Physics, 22, 4, pp. 372-375, 1951.
26. Campbell, W. B., Diffusion Rate and Activation Energy of Helium through Single and Polycrystalline Alumina, Unpublished M.S. Thesis, Georgia Institute of Technology, 1960.
27. Hayes, D., Budworth, D. W., Roberts, J. P., Permeability of Ceramics to Gas at High Temperatures, Progress Reports 1 through 7, Ceramics Division, Houldsworth School of Applied Science, University at Leeds, 1960.
28. Kingery, W. D., Oishi, Y., "Self Diffusion of Oxygen in Single and Polycrystalline Alumina," Journal of Chemical Physics, 33, 2, pp. 480-486, 1960.
29. Crandall, W. B., The Mechanical Properties of Ultra-fine Hot Pressed Alumina, State University of New York, College of Ceramics, Alfred University, 1960, 24 pp.
30. Lucalox, A New Ceramic, General Electric Research Laboratory, Schenectady, New York, 1959, 4 pp.
31. Hayes, op. cit., Progress Report No. 4.
32. Lucalox, op. cit., p. 2.
33. Campbell, op. cit., p. 22.
34. Barrer, op. cit., pp. 4-5.

35. Scheuplein, R. J., and Gibbs, P., "Surface Structure in Corundum: I. Etching of Dislocations," Journal of the American Ceramic Society, 43, 9, 1960, pp. 458-472.
36. Kriegel, W. W., Private communication to W. E. Moody.
37. Moody, W. E., Whitehead, W. D., and Kriegel, W. W., "Activation Energy for Diffusion of ¹³³Xe through MgO-Ni Cermet Compacts," Journal of the American Ceramic Society, 43, 12, 1960, pp. 634-640.
38. Campbell, op. cit., pp. 53-54.
39. Ibid., pp. 37-38.
40. Linder, R., Crosspoint Transistor Permeability of Ceramic, Bell Telephone Laboratories, 57-2525-18, 1957.
41. Moody, et al., op. cit., p. 640.

APPENDIX A

SENSITIVITY CALIBRATION AND FLOW RATE DETERMINATION

FOR A VEECO MODEL MS-9A MASS SPECTROMETER

Sensitivity Calibration

A Veeco model SC-4 Sensitivity Calibrator was used to determine the helium sensitivity of the mass spectrometer. The calibrator consisted of a helium filled metal cylinder with a glass window through which the helium diffused at a known rate. The Sensitivity Calibrator value changed at a rate of less than 0.5% per year, under constant use. Eq. (29) was used to determine the Sensitivity, or smallest detectable flow, calibrated to standard conditions of temperature and pressure.

$$\text{Sensitivity} = \frac{0.01 \times \text{Sensitivity Calibrator flow rate (atom sec.}^{-1}\text{)}}{\text{Leak Meter reading}} \quad (29)$$

Flow Rate Determination

The meter reading was converted to an S.T.P. flow rate with the use of the following equation:

$$\text{Unknown Leak Rate} = \frac{\text{Meter reading of unknown leak} \times \text{Sensitivity Calibrator flow rate (atom sec.}^{-1}\text{)}}{\text{Sensitivity Calibrator meter reading}} \quad (30)$$

APPENDIX B

DATA AND CALCULATIONS FOR SERIES J

Table 10. Series J. Polycrystalline Specimen 51 Day Run

Barrier Thickness = 0.1803 cm. Barrier Area = 0.3173 cm.²

Date	Time (Hours)	Crystal Temperature °C	Leak Meter Reading	Sensitivity Calibrator Meter Reading	Specimen Leak Rate Atoms sec. ⁻¹	C ₁ at Crystal Temperature	D* (cm. sec. ⁻¹)	Remarks
11-22	1200 to 1600	274	0.020	3.20	5.53x10 ⁹	---	---	Base line and degas
		"	"	"	"	---	---	
11-23	1030	449	0.010	"	2.76x10 ⁹	---	---	---
	1130 to 2000	480	---	"	---	9.80x10 ¹⁸	---	Admit helium
		"	0.020	3.9	5.55x10 ⁹	"	3.22x10 ⁻¹⁰	---
11-24	1200 to 1700	476	"	3.35	5.28x10 ⁹	"	3.06x10 ⁻¹⁰	---
		"	"	3.29	5.41x10 ⁹	"	3.14x10 ⁻¹⁰	---
	1745	"	"	3.20	5.52x10 ⁹	"	3.20x10 ⁻¹⁰	---
11-25	1050 to 1600	474	"	3.09	5.72x10 ⁹	9.81x10 ¹⁸	3.32x10 ⁻¹⁰	---
		"	"	"	"	"	"	---
11-26	1125 to 1700	"	0.018	3.10	5.12x10 ⁹	9.81x10 ¹⁸	2.95x10 ⁻¹⁰	---
		"	"	"	"	"	"	---
	1730	"	---	---	---	---	---	He out, boost temperature
11-27	---	---	---	---	---	---	---	"

Table 10 (Continued)

Date	Time (Hours)	Crystal Temperature °C	Leak Meter Reading	Sensitivity Calibrator Meter Reading	Specimen Leak Rate Atoms sec. ⁻¹	C ₁ at Crystal Temperature	D* ² (cm. sec. ⁻¹)	Remarks
11-28	1530	625	0.010	3.15	2.81x10 ⁹	---	---	Base line
	1625	600	"	"	"	---	---	---
	1630	615	"	"	"	8.26x10 ¹⁸	1.94x10 ⁻¹⁰	Admit helium
11-29	0945	"	"	3.14	2.82x10 ⁹	"	1.95x10 ⁻¹⁰	---
	1500 to	"	"	"	"	"	"	---
	1730	"	"	"	"	"	"	---
11-30	1345	618	0.013	3.00	3.84x10 ⁹	8.23x10 ¹⁸	2.65x10 ⁻¹⁰	---
12-1	1130 to	"	0.015	2.95	4.50x10 ⁹	"	3.10x10 ⁻¹⁰	---
	1700	"	"	"	"	"	"	---
12-2	1300 to	615	0.018	3.04	5.23x10 ⁹	8.26x10 ¹⁸	3.59x10 ⁻¹⁰	---
	1700	"	"	"	"	"	"	---
12-3	1600 to	"	0.022	3.08	6.31x10 ⁹	"	4.34x10 ⁻¹⁰	---
	2400	"	"	"	"	"	"	---
12-4	1000	"	"	3.14	6.20x10 ⁹	"	4.31x10 ⁻¹⁰	---
	1002	---	---	---	---	---	---	Helium out Boost temperature

Table 10 (Continued)

Date	Time (Hours)	Crystal Temperature °C	Leak Meter Reading	Sensitivity Calibrator Meter Reading	Specimen Leak Rate Atoms sec. ⁻¹	C ₁ at Crystal Temperature	D* (cm. sec. ⁻¹)	Remarks
12-5	1500	677	0.030	3.00	88.5×10^9	---	---	Boost temp.
12-6	0900 to	682	0.022	3.15	6.19×10^9	---	---	---
	1400	685	0.020	"	5.70×10^9	---	---	---
	1500	715	"	3.12	5.69×10^9	7.44×10^{18}	4.81×10^{-10}	Admit helium
	1815	"	0.022	3.09	6.30×10^9	"	6.34×10^{-10}	---
12-7	0940	715	0.028	2.98	8.32×10^9	7.44×10^{18}	6.25×10^{-10}	---
	1000 to	"	"	3.02	8.20×10^9	"	"	---
	1600	"	"	"	"	"	"	---
12-8	---	---	---	---	---	---	---	Standby
12-9	---	---	---	---	---	---	---	---
12-10	1020	721	0.035	3.24	9.56×10^9	7.39×10^{18}	7.35×10^{-10}	---
12-11	0900 to	723	0.045	2.93	1.30×10^{10}	7.35×10^{18}	9.90×10^{-10}	---
	1600	"	"	"	"	"	1.03×10^{-9}	---
	1700	"	"	3.05	"	"	"	Helium out Boost temp.
12-12	1000	---	---	---	---	---	---	---
12-13	0900	---	---	---	---	---	---	Power failure

Table 10 (Continued)

Date	Time (Hours)	Crystal Temperature °C	Leak Meter Reading	Sensitivity Calibrator Meter Reading	Specimen Leak Rate Atoms sec. ⁻¹	C ₁ at Crystal Temperature	D* (cm. ² sec. ⁻¹)	Remarks
12-14	0950	784	0.034	2.85	1.06×10^{10}	---	---	---
12-15	---	---	---	---	---	---	---	---
12-16	---	---	---	---	---	---	---	Standby
12-17	1330 to 1555	789 "	0.020 "	2.95 "	6.00×10^9 "	---	---	Establish Baseline
12-18	1600 1700 0945 1500 to 1700	810 " " " "	" 0.022 0.030 0.041 "	2.93 " 2.95 3.02 "	6.04×10^9 6.75×10^9 9.00×10^9 1.21×10^{10} "	6.75×10^{18} 6.75×10^{18} " " "	5.00×10^{-10} 5.68×10^{-10} 7.56×10^{-10} 1.02×10^{-9} "	Admit helium --- --- --- ---
12-19	0850 to 1700	" "	0.056 "	2.99 "	1.65×10^{10} "	" "	1.38×10^{-9} "	---
12-20	0900 to 1700	811 "	0.062 "	2.97 "	1.86×10^{10} "	6.71×10^{18} "	1.56×10^{-9} "	---
12-21	0930 1200 to 1600	" " "	0.070 0.072 "	3.06 3.02 "	2.03×10^{10} 2.20×10^{10} "	" " "	1.72×10^{-9} 1.85×10^{-9} "	--- --- ---

Table 10 (Continued)

Date	Time (Hours)	Crystal Temperature °C	Leak Meter Reading	Sensitivity Calibrator Meter Reading	Specimen Leak Rate Atoms sec. ⁻¹	C ₁ at Crystal Temperature	D* (cm. sec. ⁻¹)	Remarks
12-21	2200	---	---	---	---	---	---	Power Failure
12-22	1030 to 1700	816 "	0.075 "	2.68 "	2.48×10^{10} "	6.74×10^{18} "	2.09×10^{-9} "	---
	1730	"	0.076	2.84	2.33×10^{10}	"	1.96×10^{-9}	---
	1800	---	---	---	---	---	---	Helium out
12-23	---	---	---	---	---	---	---	Standby
12-26	---	500	---	---	---	---	---	Equipment back in operation
12-27	---	880	---	---	---	---	---	---
12-28	1200	887	0.040	3.04	1.17×10^{10}	---	---	---
12-29	0855	"	"	2.99	1.19×10^{10}	---	---	---
	1100	880	0.036	2.96	1.15×10^{10}	---	---	---
	1425	"	"	"	"	---	---	---
	1430	903	0.038	"	1.17×10^{10}	6.24×10^{18}	1.04×10^{-9}	Admit helium
	1515	"	"	2.97	1.13×10^{10}	"	"	---

Table 10 (Continued)

Date	Time (Hours)	Crystal Temperature °C	Leak Meter Reading	Sensitivity Calibrator Meter Reading	Specimen Leak Rate Atoms sec. ⁻¹	C ₁ at Crystal Temperature	D* (cm. ² sec. ⁻¹)	Remarks
12-29	1730	903	0.038	2.97	1.13x10 ¹⁰	6.24x10 ¹⁸	1.04x10 ⁻⁹	---
12-30	1000	899	0.090	2.85	2.79x10 ¹⁰	"	2.54x10 ⁻¹⁰	---
12-31	1200	"	0.130	"	4.40x10 ¹⁰	"	3.68x10 ⁻⁹	---
1-1	0045 to 1100	897 "	" "	2.76 "	4.17x10 ¹⁰ "	6.26x10 ¹⁸ "	3.78x10 ⁻⁹ "	---
1-2	0940 to 1720	895 "	0.132 "	2.85 "	4.10x10 ¹⁰ "	6.27x10 ¹⁸ "	3.71x10 ⁻⁹ "	---
1-3	2200 0900 to 1600	896 "	0.135 0.134 "	" 2.84 "	4.20x10 ¹⁰ 4.30x10 ¹⁰ "	6.26x10 ¹⁸ 6.27x10 ¹⁸ "	3.80x10 ⁻⁹ 3.90x10 ⁻⁹ "	---
1-4	1030 to 1445 1450	895 " ---	0.137 " ---	3.07 " ---	3.98x10 ¹⁰ " ---	" " ---	3.60x10 ⁻⁹ " ---	---
1-5	---	---	---	---	---	---	---	Helium out Filament burn out

Table 10 (Continued)

Date	Time (Hours)	Crystal Temperature °C	Leak Meter Reading	Sensitivity Calibrator Meter Reading	Specimen Leak Rate Atoms sec. ⁻¹	C ₁ at Crystal Temperature	D* (cm. ² sec. ⁻¹)	Remarks
1-6	---	---	---	---	---	---	---	Boost temp.
1-7	1115 to	962	0.055	2.82	1.73x10 ¹⁰	---	---	---
	1555	971	"	2.77	1.76x10 ¹⁰	---	---	---
	1600	991	---	---	---	---	---	Admit helium
1-8	0845 to	988	0.145	2.66	4.83x10 ¹⁰	5.90x10 ¹⁸	4.74x10 ⁻⁹	---
	1700	"	"	"	"	"	"	---
1-9	1000 to	983	0.175	2.74	5.66x10 ¹⁰	5.84x10 ¹⁸	5.50x10 ⁻⁹	---
	1700	"	"	"	"	"	"	---
1-10	0900 to	978	0.180	2.66	6.00x10 ¹⁰	5.85x10 ¹⁸	5.82x10 ⁻⁹	---
	1600	"	"	"	"	"	"	---
1-11	0900 to	975	0.178	2.51	6.25x10 ¹⁰	5.86x10 ¹⁸	6.20x10 ⁻⁹	---
	1700	"	"	"	"	"	"	---

D* = Values of D uncorrected for instrument base line of 0.010

Standby = Standby electronics only

DIFFUSION CONSTANT CALCULATIONS

SERIES J

Specimen Bulk Density

wt. specimen in air = 8.1349 gm.

wt. specimen in Hg = 21.600 gm.

T°C of weighing = 25°C.

ρ Hg at weighing = 13.5340 gm./cm.³

Volume

$\frac{\text{wt. in air and wt. in Hg.}}{\text{density of Hg at weighing temp.}} = \text{volume of the specimen (cm.}^3\text{)}$

$$\frac{8.1349 \text{ gm.} + 21.600 \text{ gm.}}{13.5340 \text{ gm./cm.}^3} = 2.1970 \text{ cm.}^3$$

Density

$\frac{\text{wt. specimen in air}}{\text{volume of specimen}} = \text{density of specimen (gm./cm.}^3\text{)}$

$$\frac{8.1349 \text{ gm.}}{2.197 \text{ cm.}^3} = 3.703 \frac{\text{gm.}}{\text{cm.}^3}$$

The weighing was reproducible to ± 0.005 gm. or $\pm 0.12\%$.

Diffusion Coefficient Calculations

$$T_1 = 475^\circ\text{C}$$

for volume = 1 cm.³

Average leak rate above baseline = 2.89×10^9 atom/sec.

$$D_1 = \frac{(2.89 \times 10^9 \text{ atoms/sec.})(5.68 \times 10^{-1} \text{ cm.}^{-1})}{(9.80 \times 10^{18} \text{ atoms})}$$

$$= 1.68 \times 10^{-10} \text{ cm.}^2 \text{ sec.}^{-1}$$

$$T_2 = 615^\circ\text{C}$$

for volume = 1 cm.³

Average leak rate above baseline = 3.49×10^9 atom/sec.

$$D_2 = \frac{(3.49 \times 10^9 \text{ atoms/sec.})(5.68 \times 10^{-1} \text{ cm.}^{-1})}{(8.26 \times 10^{18} \text{ atoms})}$$

$$= 2.39 \times 10^{-10} \text{ cm.}^2/\text{sec.}$$

$$T_3 = 722^\circ\text{C}$$

for volume = 1 cm.³

Average leak rate above baseline = 1.013×10^{10} atom/sec.

$$D_3 = \frac{1.013 \times 10^{10} \times 5.68 \times 10^{-1}}{7.37 \times 10^{18}}$$

$$= 7.80 \times 10^{-10} \text{ cm.}^2/\text{sec.}$$

$$T_4 = 812^\circ\text{C}$$

for volume = 1 cm.³

Average leak rate above baseline = 2.04×10^{10} atom/sec.

$$D_4 = \frac{(2.04 \times 10^{10} \text{ atom/sec.})(5.68 \times 10^{-1} \text{ cm.}^{-1})}{6.75 \times 10^{18} \text{ atoms}}$$

$$= 1.72 \times 10^{-9} \text{ cm.}^2/\text{sec.}$$

$$T_5 = 896^\circ\text{C}$$

for volume = 1 cm.³

Average leak rate above baseline = 3.91×10^{10} atom/sec.

$$D_5 = \frac{3.91 \times 10^{10} \times 5.68 \times 10^{-1}}{6.27 \times 10^{18}} = 3.54 \times 10^{-9} \text{ cm.}^2/\text{sec.}$$

$$T_6 = 975^\circ\text{C}$$

for volume = 1 cm.³

Average leak rate above baseline = 5.68×10^{10} atom/sec.

$$D_6 = \frac{(5.68 \times 10^{10} \text{ atom/sec.})(5.68 \times 10^{-1} \text{ cm.}^{-1})}{5.68 \times 10^{18} \text{ atoms}} \\ = 5.50 \times 10^{-9} \text{ cm.}^2/\text{sec.}$$

Eq. (31) was evaluated for the activation energy

$$\ln D = - \frac{E_a}{k} \frac{1}{T} + \ln D_0 \quad (31)$$

Two equations in two unknowns were obtained from eq. (31) by evaluating the D and T variables at two different points on the curve.

$$\ln D_1 = - \frac{E_a}{k} \frac{1}{T_1} + \ln D_0 \quad (32)$$

$$\ln D_2 = - \frac{E_a}{k} \frac{1}{T_2} + \ln D_0 \quad (33)$$

Ea. (32) minus eq. (33) gives:

$$\ln \frac{D_1}{D_2} = - \frac{E_a}{k} \frac{(T_2 - T_1)}{(T_1 T_2)} \quad (34)$$

Series J Calculation of the Activation Energy before the Inflection Point

Employing formula (34)

$$\ln \frac{D_1}{D_2} = - \frac{E_a}{k} \frac{(T_2 - T_1)}{T_1 T_2} \quad (34)$$

$$D_1 = 2.34 \times 10^{-10}$$

$$T_1 = 888^\circ\text{K}$$

$$D_2 = 1.68 \times 10^{-10}$$

$$T_2 = 748^\circ\text{K}$$

$$\ln 1.42 = - \frac{E_a}{k} \frac{(-140)}{(888)(748)}$$

$$E_a = \frac{(0.350)(5.34)(.888 \times 10^3 \text{ }^\circ\text{K})(1.38 \times 10^{-16} \text{ erg/}^\circ\text{K})}{(1.60 \times 10^{-12} \text{ erg/ev})}$$

$$E_a = 0.143 \text{ ev}$$

after the inflection point:

$$D_1 = 5.50 \times 10^{-9}$$

$$T_1 = 1248^\circ\text{K}$$

$$D_2 = 2.39 \times 10^{-10}$$

$$T_2 = 888^\circ\text{K}$$

$$\ln \frac{D_1}{D_2} = - \frac{E_a}{k} \frac{(T_2 - T_1)}{T_1 T_2}$$

$$\ln 23.0 = - \frac{E_a}{k} \frac{(-360)}{(1248)(888)}$$

$$E_a = \frac{3.14 \times 2.46 \times 1.248 \times 10^3 \text{ }^\circ\text{K} \times 1.38 \times 10^{-16} \text{ erg/}^\circ\text{K}}{1.60 \times 10^{-12} \text{ erg/ev}}$$

$$E_a = 0.830 \text{ ev}$$

D_o was then evaluated:

$$D = D_o e^{-E_a/RT} \quad (35)$$

Eq. (35) was rearranged to solve directly for D_o .

$$D_o = D e^{E_a/RT} \quad (36)$$

For Series J after the inflection point:

$$D_o = 5.50 \times 10^{-9} e^{\frac{8.30 \times 10^{-1} \times 1.60 \times 10^{-12}}{1.38 \times 10^{-16} \times 1.248 \times 10^3}} = 5.50 \times 10^{-9} \times e^{7.73}$$

$$D_o = 5.50 \times 10^{-9} \times 2.238 \times 10^3 = 1.259 \times 10^{-5} \text{ cm}^2/\text{sec.}$$

APPENDIX C

THEORETICAL DETERMINATION OF ACTIVATION ENERGY

BY METHOD OF MOODY (41)

The potential barrier was assumed to consist of a plane of atoms with the helium atom on one side and moving to the other side during the diffusion jump. Two mechanisms were considered as shown in Figure 19.

The activation energy was assumed to be the energy required to compress the atoms and enlarge the hole in the plane of atoms to such an extent that the helium atom could pass through. It was assumed that the oxygen atoms were connected by imaginary springs with a spring constant based on Young's modulus of elasticity of Al_2O_3 .

$$\frac{\text{Force}}{\text{Area}} = Y \frac{\Delta L}{L}$$

Y = Young's modulus of elasticity, 55×10^6 lb./in.²

ΔL = change in length

L = total length

$A = \lambda^2$ where λ is the atomic diameter for oxygen,

$$\lambda = 2.64 \times 10^{-8} \text{ cm.}$$

$F = K \Delta \lambda$ where K is the imaginary spring constant

$$\frac{K \Delta \lambda}{\lambda^2} = Y \frac{\Delta L}{L}$$

$$\frac{K}{\lambda} \frac{\Delta \lambda}{\lambda} = Y \frac{\Delta L}{L}$$

$$K = Y\lambda$$

$$\text{Work} = \int_0^{\lambda/2} K x \, dx = \left[\frac{1}{2} K x^2 \right]_0^{\lambda/2}$$

$$W = \frac{1}{2} K \left[\lambda/2 \right]^2$$

$$W = \frac{K \lambda^2}{8} = \frac{Y \lambda^3}{8}$$

For compression of two atoms on a side of an edge dislocation:

$$W = 2/8(55 \times 10^6)(68944 \text{ dynes/cm.}^2/\text{lb./in.}^2)(2.64 \times 10^{-8} \text{ cm.})$$

then for an edge dislocation compression,

$$\frac{W}{\text{Helium Diameter}} = \frac{E_a \text{ for Edge Dislocation}}{\text{Distance of Oxygen Movement}}$$

$$\frac{W(\text{ev.})}{(1.86 \times 10^{-8} \text{ cm.})} = \frac{E_a}{0.1 \times 10^{-8} \text{ cm.}}$$

$$E_a = 0.2 \text{ ev.}$$

The value calculated for interstitial diffusion was 5.7 ev.

APPENDIX D

EXPLANATION OF DATA PRESENTATION

The data presented in graphical form in Figures 12 through 17 represent the average values of the temperature and the leak rate collected during the duration of each test. The points on the curves represent averaged values, usually averaged every twelve hours. Points are shown at times where helium was admitted to and removed from the system. Each time helium was admitted to the system an instantaneous temperature rise at the barrier thermocouple was observed. This was simply due to the fact that helium is a better heat conductor than vacuum and the heat from the resistor coil reached the thermocouple more easily. When helium was removed from the system, the same phenomena was noted in reverse.

Steady state readings below 400°C were uniformly ignored in the calculation of the diffusion coefficients. Erratic leak rate readings that did not correspond to the presence or absence of helium in the system lead one to the conclusion that the system contained many contaminants during the early portion of each test at low temperatures. Readings of the leak rate immediately before and after mass spectrometer failure and equipment power failures were also disregarded as being unreliable. As an example, see Figure 16.